RSC Sustainability

ROYAL SOCIETY OF CHEMISTRY

CRITICAL REVIEW

View Article Online
View Journal

Check for updates

Cite this: DOI: 10.1039/d5su00740b

MXenes and MOFs for electrochemical reduction of carbon dioxide (CO_2)

Elham Momtaz,†[a] Masoomeh Amoozadeh,†[a] Atefeh Zarepour,[b] Arezoo Khosravi,[cd] Ali Zarrabi *[e] and Siavash Iravani *[f]

The electrochemical reduction of carbon dioxide (CO_2) represents a pivotal strategy for addressing climate change, and the integration of MXenes and metal–organic frameworks (MOFs) in this domain is garnering significant attention. This review provides a comprehensive overview of the emerging roles of MXenes and metal–organic frameworks (MOFs) as advanced materials for the electrochemical reduction of CO_2. Recent advances highlight the synergistic integration of MXenes' exceptional electrical conductivity and MOFs' tunable porosity and active sites, leading to enhanced catalytic activity, selectivity, and stability. Innovative composite architectures, including heterojunctions and hybrid structures, have shown improved conversion efficiencies toward valuable products such as carbon monoxide and formic acid. Despite these promising developments, critical challenges remain in catalyst stability, durability, and scalability, alongside economic and environmental constraints related to complex synthesis methods and material costs. Future perspectives emphasize material design optimization through surface functionalization, machine learning-guided discovery, and environmentally benign scalable production, coupled with integration into renewable-powered electrolyzed systems. The purpose of this review is to critically evaluate the state-of-the-art MXene/MOF systems, identify bottlenecks, and outline research directions that facilitate the practical and sustainable implementation of electrochemical CO_2 conversion technologies. This work aims to guide the development of efficient, durable, and economically viable next-generation catalysts for carbon-neutral fuel and chemical production, contributing to global climate change mitigation efforts.

Received 10th September 2025
Accepted 22nd February 2026

DOI: 10.1039/d5su00740b

rsc.li/rscsus

Open Access Article. Published on 23 February 2026. Downloaded on 4/9/2026 12:13:42 AM.
This article is licensed under a Creative Commons Attribution-NonCommercial 3.0 Unported Licence.

Sustainability spotlight

The electrochemical reduction of CO_2 is a vital approach to mitigating climate change by converting greenhouse gases into valuable fuels and chemicals. This work highlights the sustainable advancement achieved through integrating MXenes—known for their exceptional electrical conductivity—and metal–organic frameworks (MOFs), which offer tunable porosity and active catalytic sites. The synergy in MXene/MOF composites enhances catalytic activity, selectivity, and stability, enabling efficient CO_2 conversion into products like carbon monoxide and formic acid. Despite challenges in catalyst stability, scalability, and economic factors, advancements in material design, surface functionalization, and environmentally benign production methods present promising opportunities. This research aligns with the UN Sustainable Development Goals 7 (Affordable and Clean Energy), 9 (Industry, Innovation, and Infrastructure), 13 (Climate Action), and 12 (Responsible Consumption and Production), contributing to a carbon-neutral and sustainable future.

1 Introduction

The continuous rise of atmospheric CO_2 levels due to human activity poses severe environmental and societal risks, making its reduction a global imperative. Electrochemical CO_2 reduction provides a promising route to mitigate greenhouse gas emissions while producing value-added chemicals and fuels using renewable electricity. This process converts CO_2 into carbon monoxide (CO), formic acid, methane, ethylene, and other hydrocarbons, which can serve as feedstocks for industrial chemicals or carbon-neutral fuels such as methanol, diesel, and gasoline alternatives.[1–3] By integrating CO_2 conversion with renewable energy, this technology addresses both climate change mitigation and sustainable energy storage. Industrial-

[a]Department of Chemistry, University of Isfahan, Isfahan 81746-73441, Iran
[b]Department of Biology, Faculty of Arts and Sciences, Kocaeli University, 41001, İzmit, Kocaeli, Turkey
[c]Department of Genetics and Bioengineering, Faculty of Engineering and Natural Sciences, Istanbul Okan University, Istanbul 34959, Turkey
[d]Graduate School of Biotechnology and Bioengineering, Yuan Ze University, Taoyuan 320315, Taiwan
[e]Department of Biomedical Engineering, Faculty of Engineering and Natural Sciences, Istinye University, Istanbul 34396, Turkey. E-mail: alizarrabi@gmail.com
[f]Independent Researcher, W Nazar ST, Boostan Ave, Isfahan, Iran. E-mail: siavashira@gmail.com
† These authors contributed equally.

© 2026 The Author(s). Published by the Royal Society of Chemistry

Open Access Article. Published on 23 February 2026. Downloaded on 4/9/2026 12:13:42 AM.
This article is licensed under a Creative Commons Attribution-NonCommercial 3.0 Unported Licence.

scale deployment; however, requires catalysts and electrolyzer systems that are highly efficient, selective, stable, and cost-effective, operating in flow cells or gas diffusion electrodes to achieve commercial viability.[4–6] This approach offers promising solutions for carbon neutrality by coupling CO_2 conversion with renewable energy sources, contributing to climate change mitigation and sustainable industrial processes. Key challenges for large-scale deployment include improving the efficiency, stability, and cost-effectiveness of catalysts and electrolyzed systems, such as flow cells and gas diffusion electrodes, to achieve commercial viability in sectors like chemical manufacturing and fuel production.[7–9] To meet these performance requirements, recent research has focused on developing electrocatalysts with optimized reaction kinetics, selectivity, and stability while minimizing overpotentials. Strategies include catalytic surface modification, alloying, and structural engineering, as well as tuning electronic structures to stabilize reaction intermediates and suppress competing reactions such as hydrogen evolution.[10–12] Hybrid materials incorporating polymers, ionic liquids, and small organic molecules have also been explored to increase local CO_2 concentration and regulate reaction microenvironments.[13–15] Within this framework, MXenes and metal–organic frameworks (MOFs), particularly composites based on Ti_3C_2 MXene integrated with diverse MOF architectures, have emerged as promising candidates for CO_2 electroreduction, with several studies reporting improved conversion efficiency and product selectivity.[16–20]

MOFs are crystalline porous materials characterized by exceptionally high surface areas, tunable chemical compositions, and structural versatility, which make them excellent candidates for catalysis.[21] Their large porosity facilitates CO_2 adsorption and provides abundant active sites.[22] MXenes, a family of two-dimensional (2D) transition metal carbides, nitrides and carbonitrides, possess excellent electrical conductivity, hydrophilicity, and abundant surface terminations. These features enable rapid charge transfer and enhanced catalytic activity.[23] Combining MOFs with MXenes can synergistically overcome the limitations of each component, resulting in composite catalysts that exhibit improved performance in electrochemical CO_2 reduction through enhanced charge transport and increased active sites.[24,25] These enhancements originate from the strong synergistic interaction between the two components, whereby the intrinsically high electrical conductivity of MXenes compensates for the poor charge-transport properties of MOFs, enabling rapid electron transfer to catalytically active metal centers and stabilizing key reaction intermediates. At the same time, the high surface area and tunable porosity of MOFs prevent MXene restacking, increase the density of accessible active sites, and promote efficient CO_2 adsorption and diffusion. The formation of well-defined MXene/MOF heterointerfaces induces interfacial charge redistribution and electronic coupling, which optimizes the adsorption energies of intermediates such as *COOH and *OCHO, thereby lowering activation barriers and steering reaction pathways toward value-added products such as CO and formic acid. Moreover, the construction of binary and ternary heterojunctions within MXene/MOF composites further enhances catalytic activity by promoting charge separation, suppressing electron–hole recombination, and creating favorable reaction microenvironments. Collectively, these cooperative effects enable MXene/MOF composites to overcome the individual limitations of each material, resulting in superior catalytic efficiency, durability, and selectivity for CO_2 electroreduction applications.[26,27]

Despite recent advances, MXene/MOF hybrid catalysts still face critical material and operational challenges. MOFs exhibit limited electrical conductivity and chemical stability under electrochemical conditions, while MXenes require careful control of surface chemistry to prevent oxidation. Achieving scalable, cost-effective production of high-quality composites that maintain long-term selectivity and durability remains a major barrier to industrial deployment.[27–29] Besides, most of the recent reports focus on the performance of hybrid materials without directly evaluating them against their individual MXene and MOF catalysts under identical electrochemical conditions, making it difficult to clearly attribute performance enhancements to true synergistic effects. Consequently, the respective contributions of MXene conductivity, surface termination chemistry, MOF metal-node activity, and interfacial electronic interactions remain unclear. Addressing this gap requires thoroughly designed studies that directly compare single-component and hybrid catalysts to determine whether MXene–MOF composites offer genuine cooperative catalytic behavior or merely additive effects.[30–32] Future research is likely to focus on refining composite structures to maximize active site accessibility and electronic interactions, enhancing stability under realistic operating conditions, and integrating these materials into flexible and scalable devices powered by renewable energy. Machine learning and high-throughput screening may accelerate the discovery of optimal MXene/MOF combinations, while mechanistic insights at the atomic scale will guide the rational design of next-generation catalysts.[19,24,33–35] Enhanced understanding of reaction pathways and intermediate stabilization at the atomic scale will also guide the rational design of next-generation catalysts. Altogether, MXenes and MOFs represent a dynamic frontier with the potential to advance carbon-neutral fuel and chemical production technologies significantly.

So far, different reviews have explored MXene- and MOF-based materials; however, their scope differs markedly from that of the present work. For instance, a recent review mainly addressed synthesis strategies and broad applications, with only limited attention to electrochemical CO_2 reduction and little mechanistic discussion.[29] In contrast, this review is dedicated specifically to electrochemical CO_2 reduction, offering a focused analysis of catalytic activity, selectivity, durability, and the mechanistic roles of active sites, charge transfer, and interfacial effects in MXenes, MOFs, and their hybrid systems. Another review article critically examined MXenes as standalone electrocatalysts, focusing on surface chemistry, theoretical predictions, and intrinsic limitations.[36] In contrast, the present review expands this perspective by incorporating MOFs and MXene–MOF hybrid systems, emphasizing synergistic interfacial effects, improved intermediate stabilization, suppression of

© 2026 The Author(s). Published by the Royal Society of Chemistry

Open Access Article. Published on 23 February 2026. Downloaded on 4/9/2026 12:13:42 AM.
This article is licensed under a Creative Commons Attribution-NonCommercial 3.0 Unported Licence.

hydrogen evolution, and practical considerations such as scalability, durability, and electrolyzed integration. By integrating mechanistic insights with considerations for technological integration and renewable-powered systems, this review aims to guide researchers toward efficient, sustainable, and scalable CO_2 conversion strategies, thereby contributing to the transition toward a carbon-neutral economy.

2 MXenes in electrochemical reduction of CO_2

Since their discovery in 2011, MXenes have garnered significant attention as efficient catalysts. These 2D materials, characterized by their unique layered structure and abundant functional moieties, offer a large active surface area, which is advantageous for catalytic applications.[37–40] Their distinctive properties result from the combination of the beneficial characteristics of metals and ceramics. From metals, they inherit high electrical conductivity, while from ceramics, they gain low density, high hardness and excellent corrosion resistance.[41] One of the interesting fields of application of these compounds is their usage in CO_2 reduction[36,42,43] that results from their exceptional mechanical properties, high electrical conductivity, and distinct optical characteristics. The flexible surface chemistry and internal structure of MXenes provide a versatile platform for tailoring the binding conformations and strengths of intermediates, enabling precise modulation of their catalytic activity.[44] This tunability makes MXenes highly effective as active and selective catalysts for CO_2 reduction.

2.1 Structural characteristics of MXenes

The specific structure of MXenes can significantly affect their catalytic efficiency.[45] MXenes are among the latest additions to the family of two-dimensional materials, comprising transition metal carbides, nitrides, and carbonitrides. These materials follow the general formula $M_{n+1}X_nT_x$ ($n = 1$–3), where M denotes an early transition metal, n indicates the number of metal layers, X represents either a carbon or nitrogen atom, and T stands for the surface functional group (–O, –OH, or –F).[46,47] Transition metals play a crucial role in the catalytic activity of MXenes. Their partially filled d orbitals enable participation in bonding, stabilization of intermediates, and facilitation of electron transfer-essential mechanisms in catalytic processes.[48] Some MXenes contain more than one transition metal (M′), and the specific ordering of transition metals within the MXene structure can affect their catalytic activity. MXenes can exhibit different structural configurations based on the arrangement of M elements. They may contain a single transition metal (mono-transition metal MXenes) or multiple transition metals. When two or more transition metals are incorporated, they are classified based on their elemental distributions into two structural categories: disordered solid solution structure and ordered diatomic structure. In solid solution MXenes, multiple elements are randomly distributed within the transition metal layers, whereas in ordered diatomic MXenes, the transition metals are organized in an orderly manner. Ordered structure can be further classified into out-of-plane ordered MXenes (o-MXene) and in-plane ordered MXenes (i-MXene). In out-of-plane ordering, two transition metals are arranged such that one occupies the external layers while the other fills the central layers. In contrast, in in-plane ordering, different elements are systematically arranged within the basal plane. Additionally, some MXene structures contain vacancies, which may be distributed in either a random or ordered manner within the MXene lattice. A schematic representation of MXene structures is provided in Fig. 1.[49–51] By regulating key internal structures, such as vacancy distribution and component arrangement, the catalytic activity sites of MXenes can be fine-tuned, optimizing their overall catalytic performance. The surface chemistry of MXenes plays a crucial role in determining their chemical, physical, and electrical properties, particularly their catalytic activity and CO_2 reduction selectivity.[48,52]

2.2 Electrochemical behavior and activity

Since their discovery in 2011, MXenes have been employed as catalysts, not only for CO_2 reduction but also across various fields, owing to their high electrical conductivity and hydrophilicity. Significant research on CO_2 reduction using MXenes has been conducted, particularly since 2016.[53–56] Electrochemical CO_2 reduction refers to the conversion of CO_2 into valuable products using electricity. Materials utilized as electrocatalysts for CO_2 reduction must exhibit high electrical conductivity and a strong ability to absorb CO_2, as electricity serves as the driving force for the reaction. In the cathodic half-reaction, CO_2 is transformed into value-added chemicals through electron consumption. MXenes, with their high electrical conductivity and large exposed surface area, show great promise as catalysts for CO_2 reduction.[57]

The electrochemical catalytic activity of MXenes originates from the transition metals present on MXenes' surface and the central innermost transition-metal layer, which, through octahedral-coordination, accelerates electron transfer. Terminal metals on the MXene surface are reactive due to their vacant d-like electron shells, making them highly suitable for gas molecule capture and catalytic activity.[58,59] Capturing CO_2 using MXene is essential for facilitating electrochemical reduction. Due to their stacked structure, MXenes possess a high interlayer spacing, providing a suitable environment for CO_2 adsorption. Additionally, functional groups present on MXene surfaces enhance the adsorption of gases like CO_2.[18,60,61] The electrochemical reduction of CO_2 at MXene-electrolyte interfaces occurs in three critical phases: (a) chemical adsorption of CO_2 on the MXene surface, cleavage of C–O bonds in CO_2, and formation of C–H bonds. (b) Electron transfer and/or proton migration. (c) Desorption of product species from the electrode surface and diffusion into the electrolyte.[44]

A study investigated the electrochemical reduction of CO_2 using M_3C_2-type MXenes. The process began with CO_2 capture by M_3C_2 MXene *via* a chemisorption reaction. Adsorption occurred through electron transfer from carbides to terminal metals, increasing the metal's electronegativity and enabling interaction with the carbon in CO_2. Following CO_2 capture,

Open Access Article. Published on 23 February 2026. Downloaded on 4/9/2026 12:13:42 AM. This article is licensed under a Creative Commons Attribution-NonCommercial 3.0 Unported Licence.

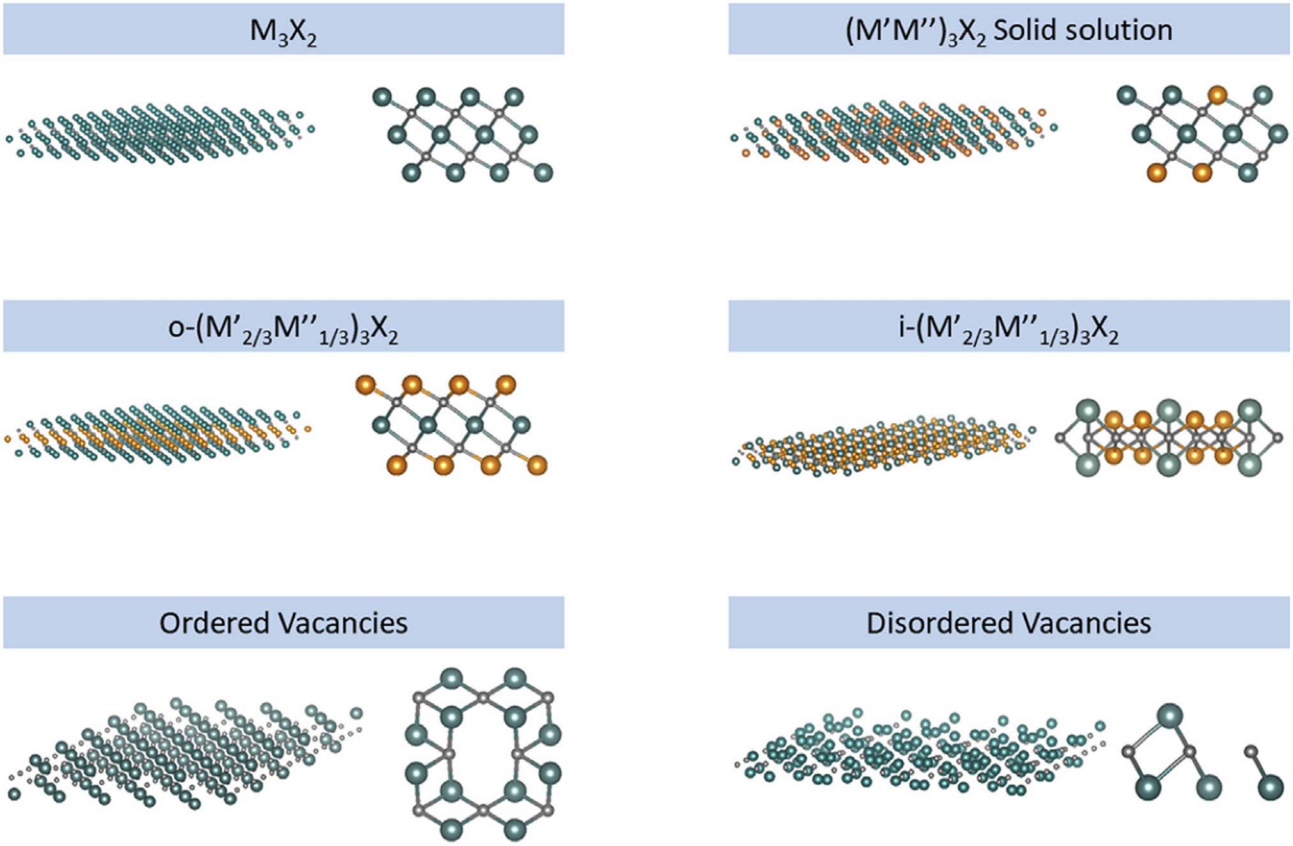

Fig. 1 Different structure of MXenes. Reprinted with permission from ref. 41. Copyright 2019, Elsevier.

activation was facilitated by modifications to the angular structure of CO_2 molecules upon interaction with Mo_3C_2, enhancing CO_2 reactivity. After activation, hydrogenation occurred, with hydrogen atoms being added to CO_2 molecules, forming intermediates that were subsequently converted to valuable products (Fig. 2).[18,59]

2.3 Recent advances in MXenes for CO_2 reduction

MXenes have emerged as promising electrocatalysts for the electrochemical reduction of carbon dioxide (CO_2RR) due to their high electrical conductivity, tunable surface chemistry, and abundant redox-active sites; however, the specific roles of the MXene components, the nature of the active sites, and the mechanisms that stabilize these sites under reaction conditions remain to be fully elucidated. The surface terminations (*e.g.*, –O, –OH, –F) and intrinsic defects of MXenes could significantly influence CO_2 adsorption and activation by modulating binding energies and facilitating charge transfer, which can direct intermediate formation (CO_2, COOH, HCOO) and product selectivity.[31,63] Computational studies further suggest that metal centers and vacancies in MXenes act as the primary active sites for CO_2 binding and reduction, and that heteroatom doping or structural modification can reduce reaction energy barriers and enhance selectivity toward specific products. However, most mechanistic insights remain theoretical, and direct experimental evidence identifying the exact active surface species under electrochemical CO_2RR conditions, as well as the dynamic evolution of these sites during catalysis, is still limited and therefore, more studies are needed in this context.[31,64]

Recent research has focused on exploiting these features to enhance the efficiency and selectivity of CO_2 reduction.[53,56] Enhancing the catalytic activity of MXenes through surface modification and heteroatom doping is a key research focus aimed at improving the electrochemical reduction of CO_2 into value-added chemicals.[65,66] Precise regulation of electronic states by optimizing the coordination environment through metal–support interactions presents a promising strategy to enhance catalytic performance. However, the effectiveness of this approach is limited by the density of functional groups on the substrate. In this context, the effect of hydroxyl (–OH) group density of MXene on the efficiency of the electrochemical CO_2 reduction reaction was investigated. In this study, $Ti_3C_2T_x$ MXene with –OH terminations was used as a support material for anchoring cobalt phthalocyanine (CoPc). A linear relationship between –OH density and catalytic performance was observed. Notably, at the highest –OH density, a faradaic efficiency of 100% was achieved within the potential range of −0.9 to −1.0 V *vs.* reversible hydrogen electrode (RHE). These findings suggest that tuning the –OH density on MXene can significantly enhance the catalytic efficiency of CoPc for CO_2 electroreduction.[67]

The strong van der Waals forces between stacked MXene layers lead to aggregation, resulting in a loss of surface area and

© 2026 The Author(s). Published by the Royal Society of Chemistry

Open Access Article. Published on 23 February 2026. Downloaded on 4/9/2026 12:13:42 AM.
This article is licensed under a Creative Commons Attribution-NonCommercial 3.0 Unported Licence.

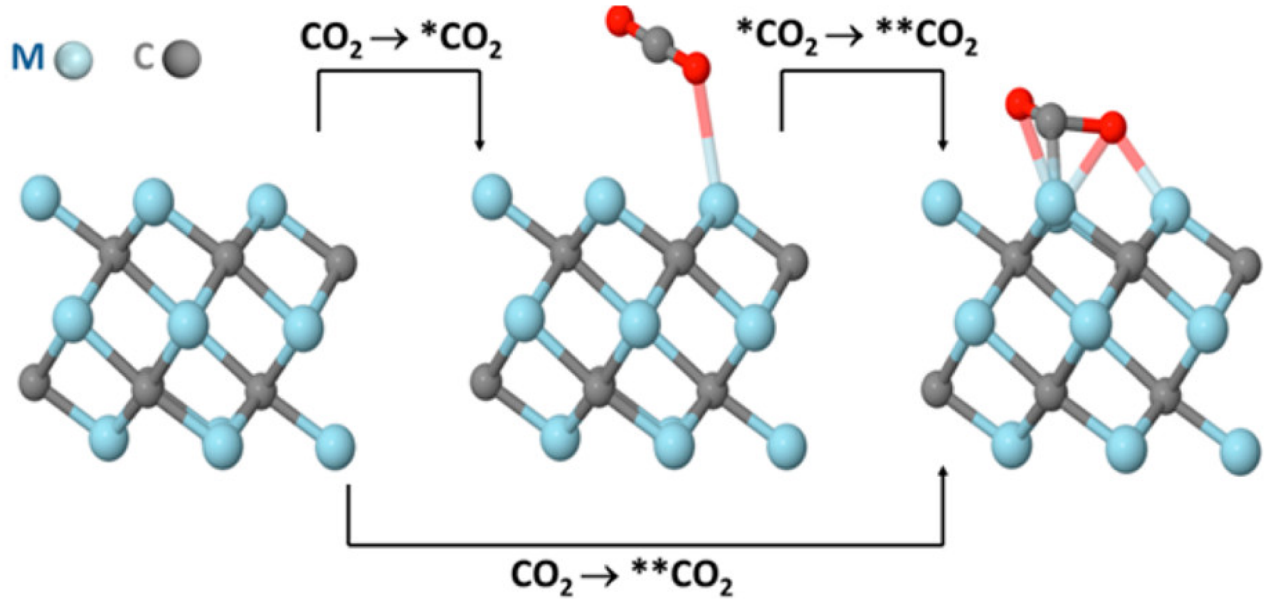

Fig. 2 The proposed route for the interaction of CO_2 with the surfaces of M_3C_2 MXene. Reprinted with permission from ref. 62. Copyright 2017, American Chemical Society.

active sites. Several approaches have been proposed to address this issue, including heteroatom doping, surface modification, and the use of interlayer spacers. To overcome this limitation, a 3D Cu–Pd/MXene aerogel was produced *via* a lyophilization process using the combination of Cu–Pd with 2D $Ti_3C_2T_x$ nanosheets. This aerogel exhibited excellent catalytic efficiency for electrochemical reduction of CO_2, achieving a faradaic efficiency of 93% and a current density of 150 mA cm^{-2}. The conversion of CO_2 to formate was accomplished with a selectivity exceeding 90%. Additionally, an overall energy efficiency of 47% was reported over five hours of operation. Thus, the careful design and modification of the MXene catalyst surface can significantly enhance the electrochemical reduction of CO_2 to formate (Fig. 3).[68]

In a computational study, the potential of MXene as an anchoring platform for transition metals in the CO_2RR was investigated. The study employed density functional theory (DFT) to explore a range of transition metals, including 3d (Sc, Ti, V, Cr, Mn), 4d (Y, Zr, Nb, Mo), and 5d (Hf) elements, as single-atom catalysts supported on oxygen-terminated Ti_2CO_2 MXene (denoted as TM@ Ti_2CO_2). The most stable configuration was found when the transition metal atom was positioned above the carbon atom in the MXene structure. A strong correlation was observed between the adsorption energy and several chemical properties, including average bond distance, Bader charge, work function, and the d-electron center of the metal. The interaction between CO_2RR intermediates and the transition metal atoms anchored on MXene facilitated charge transfer from the metal to the surrounding oxygen atoms of the MXene, enhancing catalytic activity. Among the tested metals, Ti exhibited superior CO_2 reduction performance. Additionally, TM@Ti_2CO_2 structures demonstrated higher selectivity for the CO_2RR over the competing hydrogen evolution reaction. Overall, the computational results highlighted the promising potential of single-atom transition metal-anchored MXenes as efficient and selective catalysts for electrochemical CO_2 reduction.[69]

Amorphous materials often exhibit enhanced catalytic activity due to their inherent structural characteristics, such as an abundance of defects and ligand-unsaturated atoms that provide accessible active sites for catalytic reactions. However, their low electrical conductivity and stability pose challenges in catalytic applications. MXenes, with their high electrical conductivity and stability, can overcome these limitations when used as composite materials. To check this feature, a catalyst composed of MXene and an amorphous material was introduced for electrochemical CO_2 reduction to formate. The catalyst featured a core–shell structure consisting of a crystalline SnO_2 core and an amorphous SnO_x shell, supported on Ti_3C_2 MXene. This catalyst achieved CO_2 conversion to formate with a high faradaic efficiency of 93% at −1.17 V. MXene not only improved the stability and electrical conductivity of the catalyst but also amplified the Raman signal of its components, facilitating the visualization of structural transitions during the catalytic process. CO_2 interacted with the oxygen atoms in SnO_x, forming *OCHO intermediates. These intermediates subsequently desorbed from the catalyst, leading to the formation of formate through electron and proton transfer. Thus, MXenes could be considered as promising materials for promoting electrochemical CO_2 reduction to formate and tracing catalytic reaction mechanisms (Fig. 4).[70]

Electrochemical CO_2 reduction can yield a variety of products, including CO, HCOOH, CH_4, and others. Therefore, it is essential that catalysts used in this process selectively and efficiently produce a specific desired product. The design of MXene-based catalysts capable of selectively converting CO_2 to

Open Access Article. Published on 23 February 2026. Downloaded on 4/9/2026 12:13:42 AM.
This article is licensed under a Creative Commons Attribution-NonCommercial 3.0 Unported Licence.

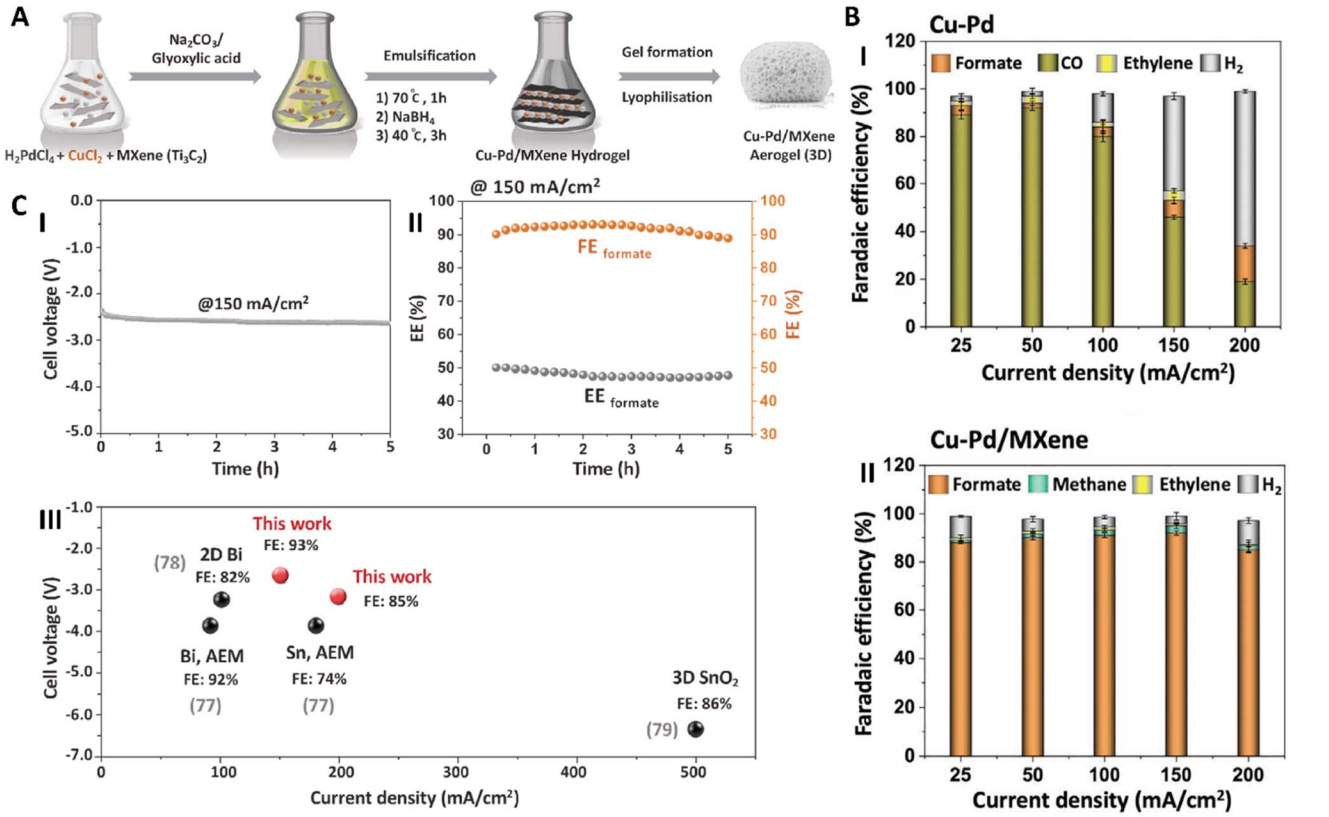

Fig. 3 (A) Schematic of Cu–Pd/MXene preparation. (B) Faradaic efficiency comparison of (I) Cu–Pd and (II) Cu–Pd/MXene at the same current density, (C) (I) long-term stability studies of Cu–Pd/MXene for CO_2 electroreduction carried out at 150 mA cm^{-2} for 5 h. (II) The faradaic efficiency of CO_2 electroreduction to formate. (III) Comparison of our work with previously published literature benchmarks. Reprinted from ref. 68 under the terms of the Creative Commons CC BY license. Copyright 2023, Willey.

targeted products has become the major focus of current research. Recently, several studies have explored the selective production of specific products from CO_2 electroreduction using MXene-based catalysts. Cao *et al.* designed a MXene-based catalyst for the electrochemical reduction of CO_2 to CO with high selectivity. The structure of $Ti_3C_2T_x$ MXene was modified through sulfur doping, where sulfur substituted oxygen functional groups on the MXene, providing anchoring sites for Zn metal (Zn-S-MXene). This unique structural modification enhanced CO_2 activation. The Zn-S-MXene catalyst demonstrated improved electrochemical CO_2 reduction to CO, achieving a faradaic efficiency of 89.7% at −0.9 V_{RHE}. Over a 20-hour period, the catalyst exhibited a minimal decrease in current density (0.5 mA cm^{-2}), while selectivity declined only slightly to 65%. Thus, this study demonstrated that modifying the MXene structure can effectively enhance the selectivity of electrochemical CO_2 reduction, enabling the targeted production of CO (Fig. 5).[71]

A ZnO-MXene nanocomposite catalyst was developed for the electrochemical reduction of CO_2 to CO and CH_4. By tuning the ZnO : MXene ratio, product selectivity could be directed toward either CO or CH_4. The catalyst demonstrated high selectivity for CH_4 with a faradaic efficiency of 79.3% at −0.56 V *vs.* RHE, and for CO with a faradaic efficiency of 76.8% at −0.78 V *vs.* RHE, while effectively suppressing the competing hydrogen evolution. Additionally, modifying MXene with ZnO significantly improved the catalyst's stability, maintaining a high faradaic efficiency for CH_4 (approximately 80%) over 24 h. These results indicated that the MXene-based catalysts enable dual selectivity for CO and CH_4 with excellent long-term operational stability.[72]

The reduction of CO_2 into high-value-added hydrocarbons, particularly those with high energy density such as propane (C_3H_8), is highly valuable from an energy perspective due to propane's low global warming potential. This process is especially beneficial when achieved through electrochemical reduction under mild conditions utilizing renewable electricity. A performed electrochemical CO_2 reduction was applied to propane using MXenes. A rational hybrid structure of Cu_2O was incorporated into $Ti_3C_2T_x$ (Cu_2O/MXene) to facilitate the conversion of CO_2 into multi-carbon products, with a particular focus on propane. The results demonstrated that this catalyst successfully converted CO_2 to C_3H_8 with a faradaic efficiency of 3.3% at −1.3 V in an aqueous electrolyte. Furthermore, the current density of Cu_2O/MXene increased in a CO_2-purged electrolyte compared to argon (Ar)-purged electrolyte. Mechanistic analysis revealed the key steps and crucial intermediates involved in propane production *via* Cu_2O/MXene. Initially, CO_2 was adsorbed onto Cu_2O/MXene, forming *COOH. This intermediate underwent dehydration, producing *CO. The *CO

© 2026 The Author(s). Published by the Royal Society of Chemistry

Open Access Article. Published on 23 February 2026. Downloaded on 4/9/2026 12:13:42 AM.
This article is licensed under a Creative Commons Attribution-NonCommercial 3.0 Unported Licence.

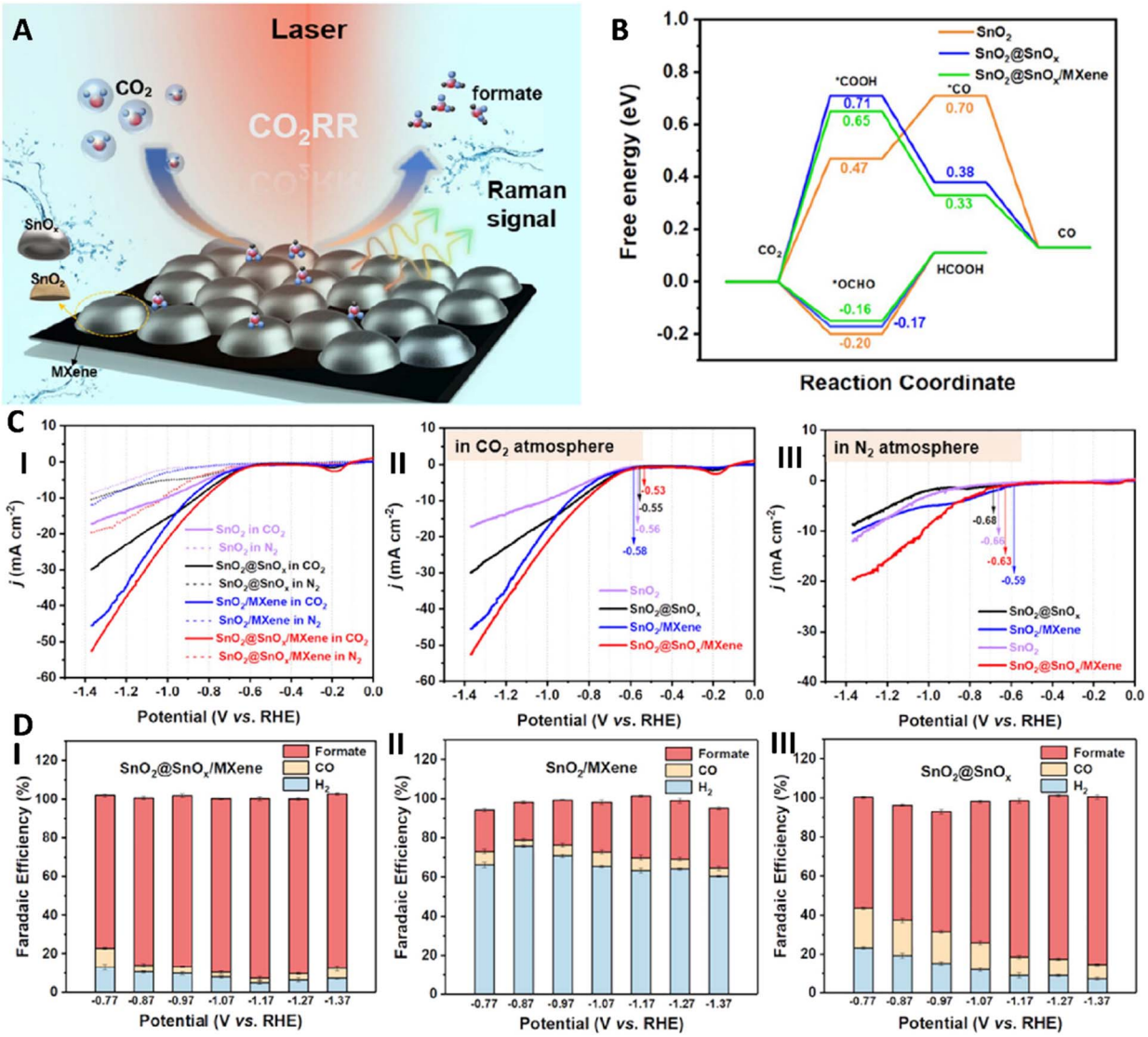

Fig. 4 (A) Schematic illustration of CO_2 electroreduction by SnO_2@SnO_x/MXene. (B) Free energy diagrams for $HCOO^-$ and CO, (C) (I–III) linear sweep voltammetry (LSV) curves of SnO_2, SnO_2@SnO_x, SnO_2/MXene, and SnO_2@SnO_x/MXene in N_2- and CO_2-saturated 0.5 M $KHCO_3$. (D) Potential-dependent faradaic efficiencies of $HCOO^-$, CO, and H_2 for (I) SnO_2@SnO_x/MXene, (II) SnO_2/MXene, and (III) SnO_2@SnO_x. Reprinted with permission from ref. 70. Copyright 2023, American Chemical Society.

species subsequently dimerized to form *OCCO on Cu_2O. The resulting *OCCO intermediate was further hydrogenated to *OCCOH, which serves as the essential precursor for generating C_2 and C_3 hydrocarbons. Finally, hydrogenation of the C_3 intermediate led to the formation of propane.[73]

The ZnO/MXene-based catalyst was produced in a study to electrochemically reduce CO_2 to CO. A stacked structure of N-doped $Ti_3C_2T_x$ was employed as the supporting material for ZnO (ZnO/N-$Ti_3C_2T_x$). The catalyst demonstrated high catalytic activity for electrochemical CO_2 reduction, achieving a faradaic efficiency of 94.4% at −0.967 V, with a current density of 7.2 mA cm^{-2}. ZnO served as the active site for CO_2 electroreduction, while MXene enhanced textural properties and electrical conductivity, facilitating efficient CO_2 mass transfer and electron transport to ZnO.[74]

Gold nanoparticles (Au) were composited with $Ti_3C_2T_x$ MXenes (Au/$Ti_3C_2T_x$) to enhance the catalytic efficiency of Au in electrochemical CO_2 reduction to syngas. This binary system was designed such that MXene served as both a substrate and a secondary catalyst, while Au functioned as the primary electrochemical reduction catalyst. The composite exhibited superior catalytic activity compared to Au and MXene individually, with the electrode achieving a current density of 17.3 mA cm^{-2} at a potential of −0.42 V. Additionally, a faradaic efficiency of 48.3% was observed in a CO_2-saturated medium. Furthermore, Electrochemical Impedance Spectroscopy (EIS) analysis demonstrated that the composite had a low charge transfer resistance compared to Au and MXene alone. Thus, the incorporation of noble metals into MXene composites can enhance electrocatalytic CO_2 reduction activity for syngas production.[75]

© 2026 The Author(s). Published by the Royal Society of Chemistry

Open Access Article. Published on 23 February 2026. Downloaded on 4/9/2026 12:13:42 AM.
This article is licensed under a Creative Commons Attribution-NonCommercial 3.0 Unported Licence.

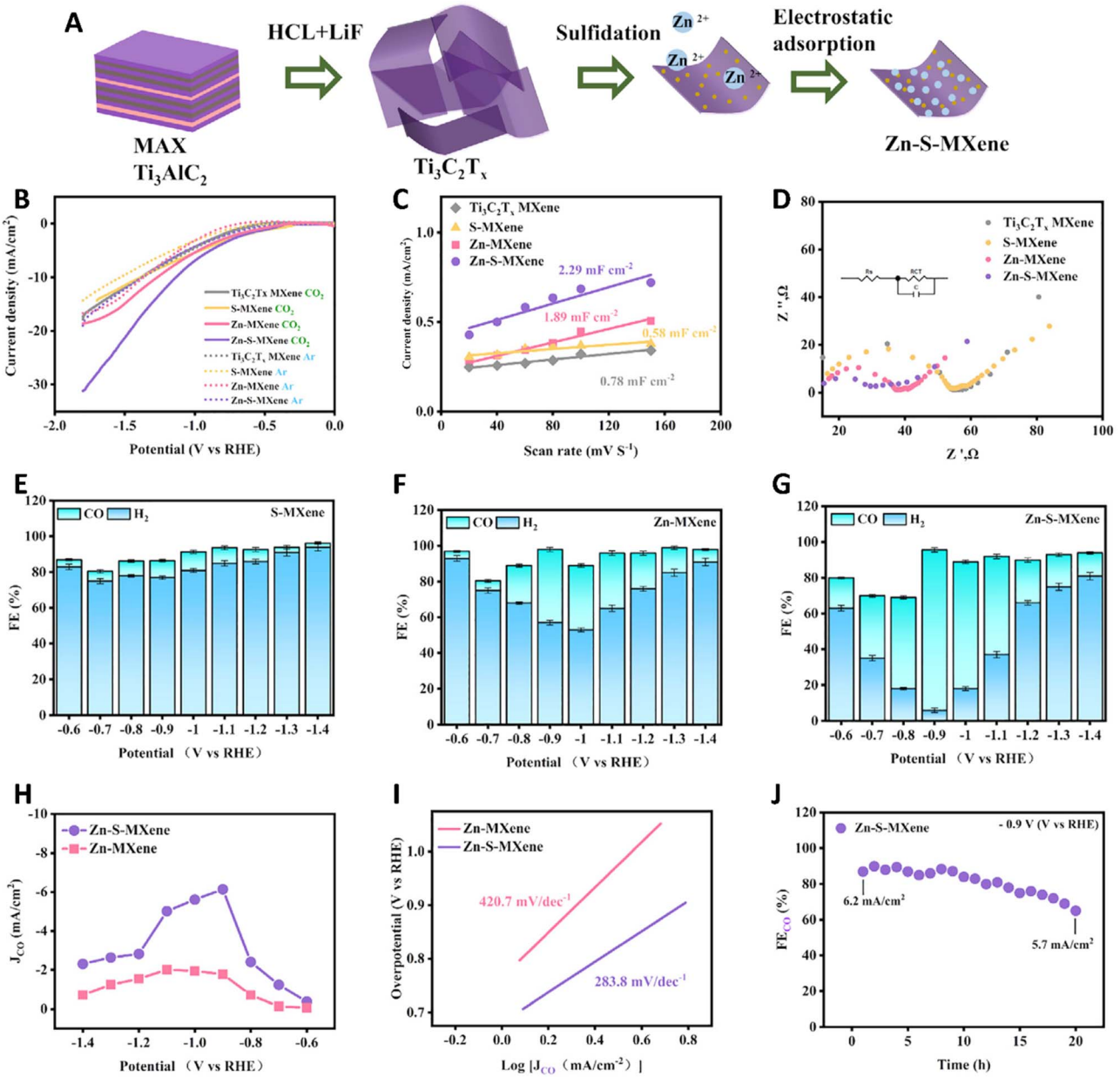

Fig. 5 (A) Synthesis path diagram of Zn-S-MXene. (B) LSV curves under different atmospheres. (C) The capacitance of the double layer is measured from the cyclic voltammetry curve. (D) Impedance test curve. (E–G) Faraday efficiency of product S-MXene, Zn-MXene, and Zn-S-MXene at different voltages. (H) Partial current density of CO. (I) The Tafel slope of the catalyst. (J) Zn-S-MXene stability test at a fixed voltage. Reprinted with permission from ref. 71. Copyright 2025, Wiley.

Beyond $Ti_3C_2T_x$, other types of MXenes were also used for the electrochemical reduction of CO_2, which are summarized in the following table (Table 1).

MXenes have emerged as highly promising materials for the electrochemical reduction of CO_2 due to their unique combination of high electrical conductivity, tunable surface functionalities, and structural versatility. Modifying MXenes through surface functionalization, heteroatom doping, and the incorporation of metal catalysts has been shown to significantly improve the activity, selectivity, and stability of CO_2 reduction reactions. Strategies such as increasing –OH termination density, creating composite aerogels, anchoring single-atom catalysts, and integration with amorphous or noble metal components have all demonstrated remarkable enhancements in faradaic efficiency and product specificity. Importantly, these modifications enable selective production of value-added products including CO, formate, methane, and even propane. Computational studies further support the potential of MXene-based platforms in tuning electronic properties for optimal catalytic performance. Overall, the rational design and engineering of MXene-based electrocatalysts offer a powerful pathway toward efficient and selective CO_2 conversion,

© 2026 The Author(s). Published by the Royal Society of Chemistry

Open Access Article. Published on 23 February 2026. Downloaded on 4/9/2026 12:13:42 AM. This article is licensed under a Creative Commons Attribution-NonCommercial 3.0 Unported Licence.

Table 1 Application of different types of MXene-based systems for the CO_2RR

MXene system	Modification/active site	Target CO_2RR product(s)	Key mechanistic insight	Study type	Ref.
MXene-Ni-N_4-C	Axial O coordination on Ni–N_4 *via* MXene coupling	CO	MXene-induced spin polarization optimizes *COOH stabilization and lowers the energy barrier for CO formation	Exp. + DFT	76
MXene-supported SACs (general)	Single metal atoms anchored on MXene	Hydrocarbon fuels (C_1/C_2)	MXene electronic structure enables stabilization of *CO and *CHO intermediates, facilitating C–C coupling	DFT	69
MXene (various compositions)	Surface electronic tuning	CO/HCOOH	Breaking linear scaling relations between *COOH and *CO adsorption enhances intrinsic activity	DFT	56
Mo_2CS_2 MXene	Non-noble metal single-atom sites	CO/HCOOH	MXene lattice and S-termination synergistically stabilize *CO_2^- and *COOH intermediates	DFT	77
Nb_2CO_2 MXene	Metal and nonmetal surface modification	C/HCOOH	Surface termination strongly governs adsorption energies and reaction pathways	DFT	57
Mo_2C MXene	Embedded single transition-metal atoms	CO	Single-atom embedding tunes d-band center, lowering limiting potentials	DFT	78
V_2C MXene	S-terminally modified SAC	CO (C_1 products)	S-termination promotes selective *COOH formation and suppresses HER	DFT	79

contributing to sustainable energy and environmental technologies.

3 Metal–organic frameworks (MOFs) in electrochemical reduction of CO_2

The electrochemical reduction of carbon dioxide is now recognized as a suitable method for converting carbon dioxide molecules into fuels and valuable chemicals such as CO, formic acid, methanol, and hydrocarbons.[80] This method reduces the environmental impact of increasing CO_2 levels and serves as a potential energy storage mechanism.[81] However, the main challenge in carrying out the CO_2 reaction is the presence of reaction overpotentials,[82] necessitating the use of catalysts to enhance efficiency and direct conversion of CO_2 toward the desired products.[83] Among the materials explored for this purpose, MOFs have gained attention due to their high porosity, tunable architecture, and modular chemical functionality, making them well-suited for CO_2 reduction applications.[84] MOFs are crystalline materials formed by organic ligands coordinating atomic centers (Fig. 6) and have numerous advantages.[85] The ability to control their structural parameters, such as pore size, synthesis approaches and morphological optimization, surface area and defect engineering, as well as the organization of metal nodes and organic ligands, are advantages of MOFs, which lead to the preparation of MOFs with high CO_2 adsorption capacity and increased electron transfer efficiency and a reduced overpotential in the CO_2RR.[86] Another advantage of MOFs is their ability to combine the advantages of homogeneous and heterogeneous catalysts.[87] In conventional homogeneous systems, the active sites are easily accessible and exhibit high activity, but their practical application is restricted due to catalyst degradation and complex separation processes.[88] Conventional heterogeneous systems are more durable than homogeneous systems, but have lower uniformity and selectivity of active sites, which limits the effective activation of CO_2.[87] MOFs effectively overcome these limitations by providing well-defined, ordered active sites in a stable and recyclable framework, which improves catalytic performance and selectivity and paves the way for the rational design of advanced electrocatalysts that balance activity, selectivity, durability, and stability.[89] Further advantages of MOFs are their extremely high surface area (5000 m^2 g^{-1}) and well-defined pore geometry.[90] Engineering the pore architecture and tuning the local catalytic environment (metal selection, ligand design, and post-synthesis modifications) can create conditions for CO_2 reduction with MOF catalysts that exhibit improved performance characteristics.[91] For instance, integrating redox-active metals, such as copper, into MOFs increases their faradaic efficiency (FE).[92]

Disadvantages of MOFs include their low conductivity and stability, which hinder their catalytic properties under practical conditions.[93] To mitigate these drawbacks and enhance MOF functionality, techniques such as pyrolysis and the formation of conductive composites are used.[94] In recent years, computational modeling has significantly advanced our understanding of the mechanisms underlying CO_2 reduction in MOF-based catalysts.[95] DFT simulations and machine learning (ML) are used to map the electronic structure of active sites and predict the adsorption energies of key reaction intermediates.[96] *In situ* spectroscopy techniques, including Infrared and Raman spectroscopy, allow real-time monitoring of reaction intermediates and provide insight into the behavior of catalysts.[97] The integration of these experimental and theoretical studies has clarified the relationship between their structural and catalytic performance properties and helped to synthesize more efficient

Open Access Article. Published on 23 February 2026. Downloaded on 4/9/2026 12:13:42 AM.
This article is licensed under a Creative Commons Attribution-NonCommercial 3.0 Unported Licence.

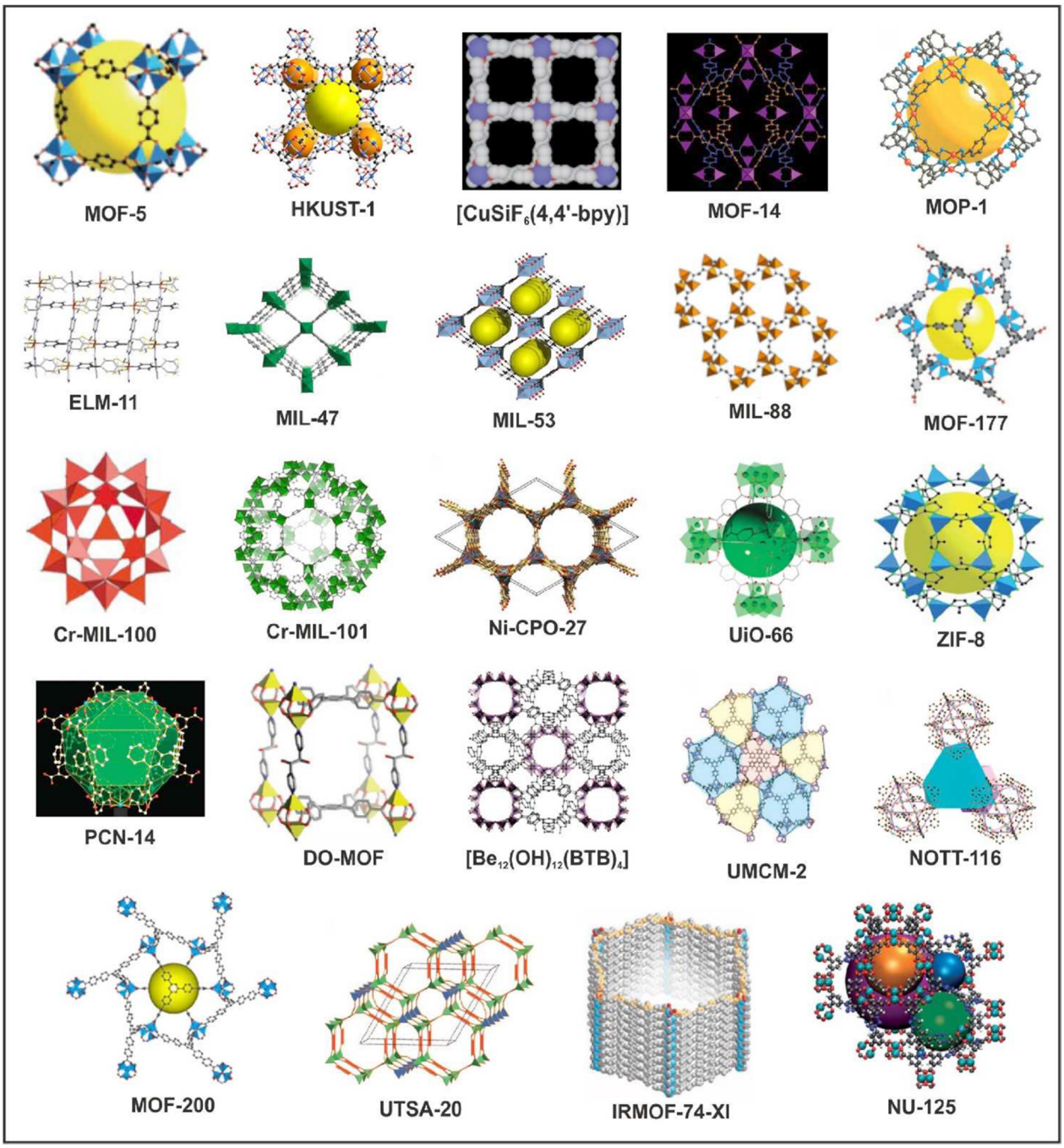

Fig. 6 Different types of MOFs with different chemical structures. Reprinted with permission from ref. 86. Copyright 2015, Royal society of chemistry.

and selective MOF-based catalysts.[98] While challenges such as electrical conductivity, scalability, and long-term durability remain with MOFs, ongoing efforts in MOF-based catalyst design, post-synthesis modifications, and computational modeling are expected to provide new perspectives for the development of optimized catalysts for CO_2 RR. In this section, we provide an overview of the structural and functional properties of MOFs, the factors limiting the conductivity and durability of MOFs, and recent advancements in the field.

3.1 Structural features of MOFs

MOFs consist of metal nodes and organic ligands,[99] where the metal nodes can be selected from a wide range of elements, including transition metals (*e.g.* iron, copper, cobalt, nickel) and lanthanides. The redox properties of the individual metals and coordination geometries influence the catalytic behavior of the resulting MOFs.[100] For example, the copper-based MOF HKUST-1, in which the copper is coordinated by benzene-1,3,5-tricarboxylate, facilitates electron transfer reactions, and

© 2026 The Author(s). Published by the Royal Society of Chemistry

Open Access Article. Published on 23 February 2026. Downloaded on 4/9/2026 12:13:42 AM. This article is licensed under a Creative Commons Attribution-NonCommercial 3.0 Unported Licence.

enabling the selective production of hydrocarbons and alcohols.[101] Common organic ligands include carboxylates, imidazolates, and pyridinates, which can be chemically modified to fine-tune their electron-donating and electron-accepting properties, thereby not only stabilizing the crystal lattice but also modulating electron transfer processes.[102] The rational design of metal–organic ligand nodes in MOFs helps to synthesize porous crystal frameworks with a high surface area for the adsorption of CO_2 and reduction.[103] MOFs have a high internal surface area, which allows more CO_2 to be adsorbed onto the structure and increases interaction with active catalytic sites.[87] The hierarchical porosity is a characteristic of MOFs, which includes ultra-micropores (about 2 nm) and mesopores (2–50 nm).[85] Carbon dioxide interacts with the micropores, increasing the local CO_2 concentrations near the active sites and promoting the formation of adsorbed intermediates such as $*CO_2^-$, *COOH, or *HCOO for CO_2 reduction.[98] Mesoporous porosity increases the molecular diffusion of the adsorbed CO_2 (fast mass transfer) and increases current density in the catalytic reaction.[104] The functional importance of this pore hierarchy is validated by targeted synthesis studies, which show that deliberately regulating pore architecture in MOF-derived catalysts is a proven strategy to boost CO_2 mass transfer and overall electrocatalytic efficacy. As a specific example, Jia *et al.* synthesized a hierarchically ordered porous single-atom Fe–N–C catalyst *via* a silica-templated method using ZIF-8 and iron salts.[105] This process resulted in an interconnected network of micropores, mesopores, and macropores that markedly improved reactant accessibility and gas diffusion. Using *operando* electrochemical impedance spectroscopy, the authors revealed that this hierarchical pore morphology drastically lowers mass transfer resistance to the isolated Fe active sites during the CO_2 reduction reaction (CO_2RR). This optimized structure led to superior performance in the mass-transfer-limited regime, achieving a maximum CO partial current density of approximately -19 mA cm^{-2} in a conventional H-cell configuration.[105] These findings underscore the critical role of synthesis-controlled pore engineering in simultaneously optimizing reactant accessibility and current density, which is a key objective in CO_2 electrocatalysis. Such hierarchical architectures are typically created by carefully tuning synthesis parameters including precursor composition, pyrolysis conditions, and the use of templating agents to control pore formation and connectivity across multiple length scales, thereby enhancing mass transport kinetics toward the catalytic active sites.[106]

The structural properties and performance of MOFs depend on their synthesis techniques and the employed morphological control strategies.[107] Traditional solvothermal and hydrothermal methods are commonly used for the synthesis of MOFs; however, these methods are associated with challenges such as high cost, scalability issues, and environmental impact due to toxic solvents and extended reaction times.[108] Therefore, green synthesis methods with the advantages of using non-toxic solvents, short reaction times, and operating under mild conditions overcome the limitations of conventional methods and reduce environmental impact and manufacturing expenses.[109]

Important synthesis parameters such as temperature, reaction time, pH, and reactant concentration influence the pore architecture and crystallinity of MOFs.[108] By tuning these parameters, highly porous structures can be produced for maximum CO_2 uptake and reduced overpotential required for CO_2 reduction reactions.[110] For example, it was demonstrated in a study that the presence of water as a stable solvent, combined with methanol as a polarity regulator, enabled better control over the size and morphology of PNU-25 crystals. The combination of water and methanol resulted in a structure with a higher specific surface area and more uniform distribution of pores for CO_2 uptake compared to the use of each solvent alone.[111] Maintaining the structural integrity of MOFs during CO_2 reduction reaction is a critical challenge, particularly under dynamic conditions such as fluctuations in applied potential, pH variations, and changes in electrolyte composition. One strategy to address this issue is the precision selection of robust metal–ligand pairs to minimize the degradation of the framework over extended reaction times.[98] Moreover, defect engineering has emerged as a promising approach to enhance MOF stability. Structural defects such as missing linkers act as additional active sites for CO_2 adsorption and increase the efficiency of CO_2 reduction. Optimizing the defect density enhances the reactivity of MOFs without compromising their durability.[112] The extensive porosity, while advantageous for applications like gas adsorption, reduces the continuous pathways for electron transport and thus reduces conductivity.[113]

In MOFs, the metal centers are linked together by organic ligands that typically restrict electron flow.[114] On the other hand, the type of functional groups present in the MOF structure can affect the conductivity of the structure, such that some groups facilitate charge transfer, but many of them hinder the movement of electrons. Since most of MOFs have inherently semiconducting behavior, structural modification or doping is required to increase their conductivity.[115] In general, the problem can be solved using methods like incorporating conjugated organic binders, developing MOF-based composites, employing post-synthesis modification techniques, and fabricating two-dimensional structures.

In summary, the structural versatility of MOFs offers significant advantages for CO_2 electrocatalysis, including ultrahigh surface area, tunable porosity, and molecularly precise active sites. However, these benefits are counterbalanced by inherent challenges such as low electrical conductivity and limited stability under operational conditions.

3.2 Tunability and functionalization

The ability of optimizing the performance of MOFs for electrocatalysis reduction of CO_2, that includes CO_2 adsorption capacity, electron density at the active sites, durability, and electron transfer efficiency, has attracted lots of attention.[116] To optimize the catalytic properties of this structure, different functionalization of the frameworks could be applied including:

3.2.1 Metal node engineering. Metal node engineering has been proposed as an important strategy to enhance the catalytic efficiency and electrocatalytic performance of MOFs. In this

Open Access Article. Published on 23 February 2026. Downloaded on 4/9/2026 12:13:42 AM.
This article is licensed under a Creative Commons Attribution-NonCommercial 3.0 Unported Licence.

context, the careful selection of the composition and oxidation state of the metal centers is essential;[117] for instance, utilizing copper based MOFs could mediate multi-electron transfer reactions.[118] Cobalt- and nickel-based MOFs favor the production of CO and formate over CO_2 reduction due to their unique redox properties.[119] Bi- and trimetallic MOFs are employed to enhance the charge transfer kinetics and selectivity. These metal frameworks increased the efficiency of CO_2 electrocatalysts by promoting the formation of additional intermediate species.[120,121] For example, the trimetallic Cu–Zn–Pd MOF achieved a faradaic efficiency of 95% for the production of CO at −0.75 V *vs.* RHE (Reference Hydrogen Electrode). The incorporation of Pd into the Cu–Zn framework increased the electrochemically active surface area, facilitated electron transfer, reduced overpotential, and enhanced current density.[120] Recent advances include post-synthetic metal exchange, in which the original metal nodes are replaced with more redox-active ions that led to enhancing both catalytic efficiency and structural stability. The replacement of nickel ions with zinc ions, for example, showed a faradaic efficiency of 71.9% for CO production and a current density of 10.48 mA cm^{-2} (Fig. 7).[122]

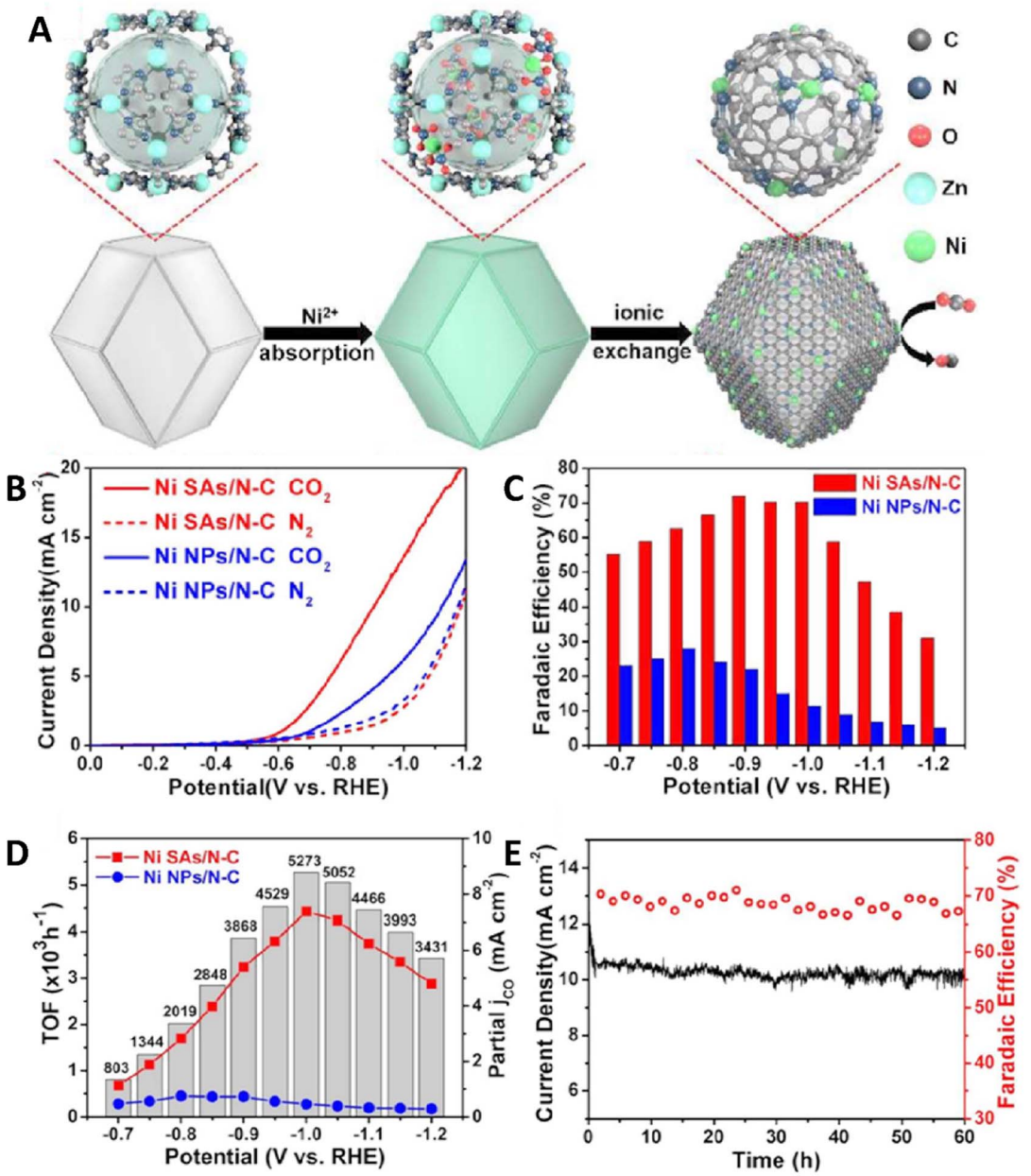

Fig. 7 (A) The schematic image of Ni SAs/N-C. (B) LSV profiles recorded in N_2-saturated (dashed lines) and CO_2-saturated (solid lines) 0.5 M $KHCO_3$ electrolyte at a scan rate of 10 mV s^{-1}. (C) Faradaic efficiencies for CO formation and (D) corresponding partial CO current densities, normalized to the geometric surface area, along with turnover frequencies (TOFs) for Ni SAs/N-C and Ni NPs/N-C measured at various applied potentials. (E) Long-term electrochemical stability of Ni SAs/N-C evaluated at −1.0 V *versus* RHE over a continuous operation period of 60 h. Reprinted with permission from ref. 122. Copyright 2017, American Chemical Society.

© 2026 The Author(s). Published by the Royal Society of Chemistry

Open Access Article. Published on 23 February 2026. Downloaded on 4/9/2026 12:13:42 AM. This article is licensed under a Creative Commons Attribution-NonCommercial 3.0 Unported Licence.

3.2.2 Organic ligand modifications. One strategy to optimize the electrocatalytic performance of MOFs is to modify the organic ligands that influence charge transfer, product selectivity, and stabilization of reaction intermediates.[123] When CO_2 is adsorbed on MOFs, electron transfer leads to the formation of *COOH and *HCOO intermediates whose stability ultimately directs the reaction toward producing either CO or formic acid.[124]

A critical element in ligand modification is the introduction of electron-donating groups (NH_2, OH) or electron-accepting groups (NO_2, CF_3) that affect the performance of the MOF structure. Electron-donating groups increase CO_2 uptake and facilitate the electrochemical reduction of CO_2, while electron accepting groups improve product selectivity.[123,125] For example, amino modifications of a cobalt-porphyrin-based MOF (H-Co-1) led to the production of a new MOF (NH_2-Co-1) that achieved a faradaic efficiency of 99.4% for the conversion of CO_2 to CO. The amine groups enhanced selectivity toward CO production by producing hydrogen bonds with CO_2 molecules and suppressing the undesirable hydrogen evolution reaction.[126]

Advancing beyond simple pendant functional groups, the strategic incorporation of inherently conjugated organic linkers such as phthalocyanines and porphyrins provides a more profound method to structurally and electronically engineer the MOF backbone.[127] These conjugated macrocycles create extended π-electron networks within the framework, facilitating long-range charge transport, enhancing electron delocalization at active sites, and thereby boosting electrocatalytic activity. This principle is demonstrated by several high-performance catalysts:

- In phthalocyanine-based systems, the conductive two-dimensional MOF NiPc-NiO_4 achieves a high CO faradaic efficiency of 98.4% and a large partial current density of 34.5 mA cm^{-2}, outperforming many non-conjugated analogues due to its efficient charge-transport network.[127] Similarly, the CoPc-Cu-O catalyst, a cobalt phthalocyanine-based MOF that is layered with copper ions to form a π-core structure, exhibited an electrical conductivity of 2.12 S m^{-1} and achieved a faradaic efficiency of 79% for CO production.[128]
- In porphyrin-based systems, the framework PCN-222(Co), synthesized *via* solvothermal method, exhibits a high CO faradaic efficiency of ∼94% with reduced charge-transfer resistance, a direct benefit of its porphyrin linker's conjugated electron system.[129]

These examples illustrate that rational ligand design, particularly using conjugated macrocycles, can fundamentally tune the electronic properties of a MOF, creating an intrinsic pathway for efficient electron transfer without relying solely on external conductive additives. Secondary interactions, such as hydrogen bonding and π–π stacking between these conjugated units, can further enhance stability and fine-tune the local environment of active sites.[130]

3.2.3 Post-synthesis modifications. Post-synthesis modification (PSM) is a method to improve the efficiency of CO_2 reduction that allows fine-tuning of the MOF structures. This strategy includes metal ion substitution, modification of covalent bonds, and incorporation of guest molecules.[131] Metal ion exchange is the selective replacement of metal nodes by controlling the oxidation state of the metal center while maintaining the overall stability of the framework.[132,133] For example, it was demonstrated that the replacement of Zn ions in Zn-based MOFs with nickel ions improved the adsorption of CO_2 and reduced the activation energy for the formation of *COOH intermediates, thereby leading to a significant increase in the faradaic efficiency of CO conversion by 95%.[133]

Covalent modification of linkers broadens catalytic versatility by introducing redox-active or protonic groups.[134,135] For example, by covalently attaching an unstable cyclic carbon (NHC) ligand to a UIO-66 framework and forming strong interactions with the metal centers, the uptake of CO_2 was facilitated and additional active sites were provided. Moreover, the protonic groups in the structure contributed to the stabilization of the key intermediate species, resulting in raising the faradaic efficiency for CO production from 50% in the unmodified structure to 80.1%.[134]

The incorporation of guest molecules, small molecules, or nanoparticles, into the pores of MOFs leads to the production of hybrid catalysts that combine the advantages of both homogeneous and heterogeneous catalysts.[136] For example, researchers integrated copper oxide (Cu_2O) nanoparticles into a MOF structure *via* incorporating nanoparticles into the pores that led to increasing the density of active sites and electron transport. Therefore, the faradaic efficiency of 79.4% was reported for the production of hydrocarbons at a potential of −1.1 V *vs.* Ag/AgCl.[137] Advanced techniques in guest encapsulation, such as single molecule trapping and ionic liquid entrapment, resulted in uniform catalytic sites and enhanced current density. For instance, the introduction of ionic liquids into the pores of HKUST-1 led to an increase in the local concentration of CO_2 and an improvement in the thermodynamics of its conversion to methane, and a faradaic efficiency of 65.5% during electrochemical reduction resulted.[138]

3.2.4 Enhancing electrical conductivity. Although MOF structures offer numerous advantages for CO_2 reduction, they exhibit inherent low conductivity due to the insulating nature of the organic bonds and the spatial separation of metal centers.[139] The search to overcome this challenge has focused on three complementary approaches: intrinsic structural engineering, the creation of composite materials, and post-synthesis modification methods. The first approach addresses the root cause through rational framework design. From a structural perspective, electrical conductivity in MOFs is governed by the intrinsic connectivity between metal nodes, the extent of π-conjugation in organic linkers, and the dimensionality of the framework rather than solely by the presence of external conductive additives.[139] Efficient charge transport pathways can be realized through extended π-d conjugation and continuous coordination bonds between metal centers and conjugated organic linkers, which create delocalized electronic networks within the MOF architecture. Such design principles have been widely discussed in the context of conductive MOFs, where strategies like incorporating planar conjugated ligands, optimizing metal–ligand orbital overlap, and constructing two-

Open Access Article. Published on 23 February 2026. Downloaded on 4/9/2026 12:13:42 AM. This article is licensed under a Creative Commons Attribution-NonCommercial 3.0 Unported Licence.

dimensional (2D) frameworks with in-plane π conjugation significantly enhance electrical conductivity and facilitate electron hopping between adjacent sites.[139,140] Therefore, tuning conductivity is not only achieved by external additives but also by rational framework design, where modifying ligand chemistry, increasing π-electron delocalization, and reducing distances between conductive pathways can markedly improve charge carrier mobility and lower charge transfer resistance in electrocatalytic CO_2 reduction.[139]

To complement these intrinsic design strategies, MOF-based composites containing highly conductive materials (graphene, carbon nanotubes, and conductive polymers) have been introduced, which utilize high porosity and chemical versatility of MOFs in combination with the excellent electron mobility of the additives, to create efficient electron highways that enhance charge transport.[141,142] In such composite electrocatalysts, the individual components are not merely mixed but play distinct functional roles that synergistically enhance activity and selectivity. Specifically, the MOF framework acts as the primary catalytic platform, providing a high density of structurally defined metal–ligand active sites that facilitate CO_2 adsorption and initial activation.[143] Meanwhile, incorporating conductive supports such as graphene or carbon nanotubes significantly enhances electron transport by forming continuous pathways between the electrode and the active centers, overcoming the inherently low conductivity of many MOFs.[143,144] Furthermore, embedding metal nanoparticles within the MOF pores introduces additional catalytic interfaces and helps stabilize key reaction intermediates (*e.g.*, ·COOH and ·HCOO) through electronic and geometric effects, while the porous MOF network prevents nanoparticle agglomeration and maintains a high dispersion of active sites.[144] Finally, the confined porous environment of MOFs also contributes to the stabilization of adsorbed intermediates *via* coordination to metal nodes and secondary interactions such as hydrogen bonding or electrostatic effects, which collectively lower overall reaction barriers and improve kinetics.[144] This cooperative interaction between the structural components and the conductive or metallic additives leads to enhanced charge transport, greater active site utilization, and significantly improved electrocatalytic performance for CO_2 reduction.[143] These conceptual strategies are validated by experimental breakthroughs. For example, integrating polypyrrole molecules into the MOF structure (MOF-545-Co) led to an enhancement in the overall electrical conductivity of material and facilitated electron transport during CO_2 reduction. The efficiency of CO production reached to about 98%, which was twice as high as the faradaic efficiency of the pure MOF.[142] Similarly, the principle of intrinsic conductivity engineering is demonstrated by modifying MOF structure with conjugated organic linkers that delocalize π-electrons and establish continuous electron pathways, thereby integrating adjacent metal centers, enhancing charge transport, lowering the overpotential required for CO_2 reduction, and improving catalytic efficiency.[145]

Further improvements can be achieved through post-synthesis modification methods, such as controlled thermal decomposition (pyrolysis), which converts MOFs into carbon-rich frameworks embedded with metal or metal oxide nanoparticles and increases conductivity while retaining the original porosity (Fig. 8).[146] In 2020, carbonized copper-based MOFs, including HKUST-1 and PCN-62, were transformed into porous Cu–C composites that used as efficient catalysts for the electrochemical reduction of CO_2 to isopropanol and delivered a partial current density of approximately 8 mA cm^{-2} for isopropanol production. The onset potential for CO_2 reduction shifted positively by around 100 mV, effectively lowering the overpotential required for the reaction. Over a one-hour period, HKUST-1 maintained at least 85% of its initial current and achieved a faradaic efficiency of 72% for converting CO_2 to isopropanol.[147]

3.3 Recent advances in MOFs for CO_2 reduction

In recent years, the electrochemical reduction of CO_2 has made significant progress thanks to the unique capabilities of MOFs.[149] Due to their tunable structural features and uniformly distributed active sites, considerable advancements have been achieved in enhancing the catalytic activity for CO_2 reduction and improving product selectivity, while eliminating challenges such as the low conductivity and limited stability of such structures.[125] To broaden the perspective beyond the most commonly studied Cu-, Co-, and Zn-based systems, several other promising MOF families have emerged. For instance, Zr-based frameworks such as UiO-66 and its derivatives are widely recognized for their exceptional structural and chemical stability under electrochemical conditions. When employed as coatings or templates, they can improve product formation and catalytic durability in CO_2RR systems.[150] Similarly, MOFs incorporating earth-abundant transition metals such as Fe and Mn provide redox-active centers that facilitate CO_2 activation and offer alternative pathways to value-added products, a trend highlighted in recent analyses of diverse transition-metal MOF catalysts.[151] In addition, porphyrinic and two-dimensional conjugated MOFs (2D c-MOFs) represent an emerging class of materials for electrocatalysis. These frameworks combine extended π-conjugated networks which grant high intrinsic electronic conductivity with well-defined active sites, offering new opportunities for efficient and selective CO_2 conversion beyond traditional systems.[129,140] These developments underscore the expanding material palette for MOF-based CO_2RR electrocatalysts and highlight opportunities for tailoring active sites, conductivity, and stability across diverse coordination environments.

Several studies have demonstrated that pristine MOFs with redox active sites such as copper, zinc, cobalt, *etc.* showed promising performance in converting CO_2 into the products like CO, methane, formic acid, or even more complex compounds. When CO_2 adsorbs onto the catalyst surface, one metal center initiates the reaction by donating an electron, converting CO_2 into a reactive radical intermediate. Rather than allowing this intermediate to remain unstable, a neighboring metal center provides a second electron or a proton, thereby accelerating the reaction and lowering the required energy. This cooperative mechanism facilitates the cleavage of strong

© 2026 The Author(s). Published by the Royal Society of Chemistry

Open Access Article. Published on 23 February 2026. Downloaded on 4/9/2026 12:13:42 AM.
This article is licensed under a Creative Commons Attribution-NonCommercial 3.0 Unported Licence.

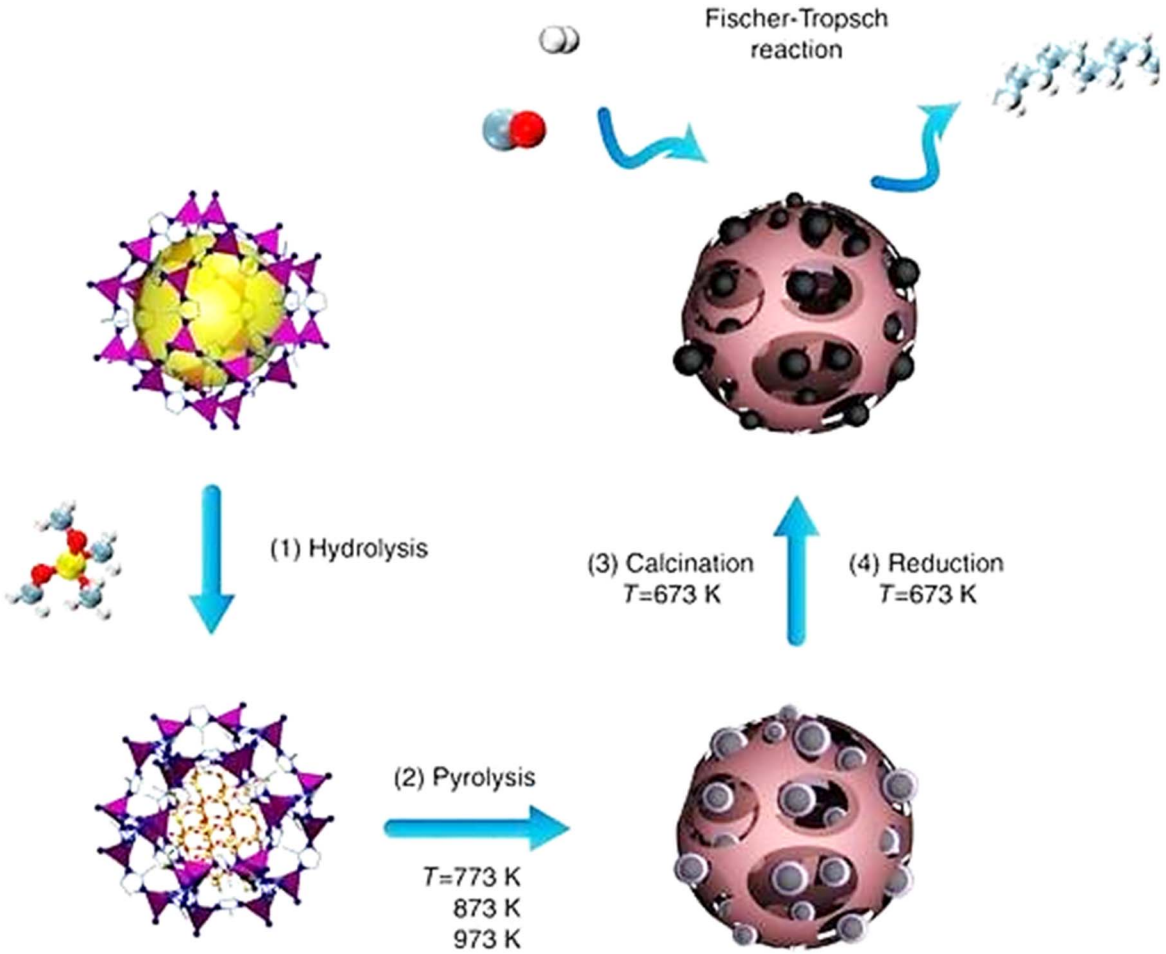

Fig. 8 The schematic illustration of MOF catalyst preparation *via* pyrolysis. Reprinted from ref. 148 under the terms of the Creative Commons CC BY license. Copyright 2017, Springer.

chemical bonds and stabilizes key intermediates throughout the process. Even more effectively, the metals often share the same surrounding environment, which spatially aligns reactive sites to facilitate efficient electron and proton transfer. The organic linkers within the framework provide an additional level of stabilization by forming hydrogen bonds that anchor reactive intermediates, thereby preventing their diffusion or participation in undesired side reactions. This well-designed architecture within MOFs enhances CO_2 activation, facilitates multi-step reaction pathways, and improves selectivity toward value-added products such as CO, formate, and hydrocarbons.[152,153]

A novel gas-diffusion electrode (GDE) was developed using CuTz-1 (a type of MOF), blended with ethanol and Nafion, and spray-coated onto a specially treated carbon paper. This creates a porous, layered structure that prevents flooding, maintaining efficient contact between CO_2, electrolyte, and the electrode, facilitating smooth movement of gases in and out during reactions, and anchored the MOF securely for long-term stability. At −0.8 V *vs.* RHE, the setup delivered 62.7% efficiency for converting CO_2 to CO, with a sustained partial current of −35.1 mA cm^{-2} over 10 h and minimal performance loss. Impedance spectroscopy showed low resistance (∼30 Ω), indicating seamless electron transport *via* molecular linkers. Capacitance measurements pointed to a very active surface area (∼12 cm^2 per 1 cm^2 of electrode), reflecting a dense network of reactive sites. Thus, these results highlight how the structured arrangement of Cu_5tz_6 clusters not only improves efficiency but also stabilizes crucial reaction intermediates, making it a standout solution for sustainable CO_2 reduction.[152]

MOF-74 frameworks were synthesized with copper and zinc using a solvothermal approach and evaluated for their efficiency in converting CO_2 to CO *via* electrochemical reduction. When subjected to LSV under CO_2 atmosphere, Cu-MOF-74 demonstrated an onset reduction potential of −0.60 V *vs.* RHE, roughly 150 mV more positive than that of Zn-MOF-74. At a fixed potential of −0.80 V *vs.* RHE, chronoamperometric measurements revealed a peak CO faradaic efficiency of 82% for Cu-MOF-74, significantly outperforming Zn-MOF-74, which achieved 45%. The copper-based MOF also maintained a stable current density of around 14 mA cm^{-1} 2 over 6 h. Tafel slope analysis indicated more favorable reaction kinetics for Cu-MOF-74, with a slope of 108 mV dec^{-1} compared to 163 mV dec^{-1} for Zn-MOF-74. Electrochemical impedance spectroscopy further

Open Access Article. Published on 23 February 2026. Downloaded on 4/9/2026 12:13:42 AM.
This article is licensed under a Creative Commons Attribution-NonCommercial 3.0 Unported Licence.

supported this, revealing a lower charge-transfer resistance of ~42 Ω for Cu-MOF-74 *versus* ~78 Ω for its zinc counterpart. Brunauer–Emmett–Teller (BET) surface area measurements showed that Cu-MOF-74 offered a larger accessible area (1450 $m^2\ g^{-1}$) compared to Zn-MOF-74 (1188 $m^2\ g^{-1}$), which correlated with its enhanced electrochemical activity. Finally, density functional theory calculations suggested that the superior performance of Cu-MOF-74 stems from a lower activation energy by 0.15 eV for the formation of the *COOH intermediate in the rate-limiting step of CO_2 reduction.[153]

To solve the problem of low electrical conductivity of MOFs, researchers have introduced conductive composite materials. A copper-based MOF (Cu-THQ) integrated with edge-functionalized graphene (EFG), showed a faradaic efficiency of 31.7% for formate production at a low voltage of −0.25 V *vs.* RHE and a current density of 3 mA cm^{-2}. Continuous operation at −0.25 V for 6 h resulted in minimal loss of current or selectivity, demonstrating stability. The enhanced conductivity and plate-like structure of EFG improved CO_2 accessibility and facilitated efficient electron transfer compared to graphene oxide, which significantly reduced both the onset potential and overpotential. Surface hydroxyl and carboxyl groups on EFG serve as anchoring sites for Cu-THQ nanoplates, preventing their aggregation and ensuring greater exposure of active sites. EIS data indicated that the Cu-THQ-EFG composite exhibited approximately half the charge-transfer resistance of the GO-supported counterpart. The near-equilibrium onset potential suggested that Cu-THQ-EFG effectively stabilized the *HCOO intermediate with minimal energy input, promoting highly selective formate production (Fig. 9).[154]

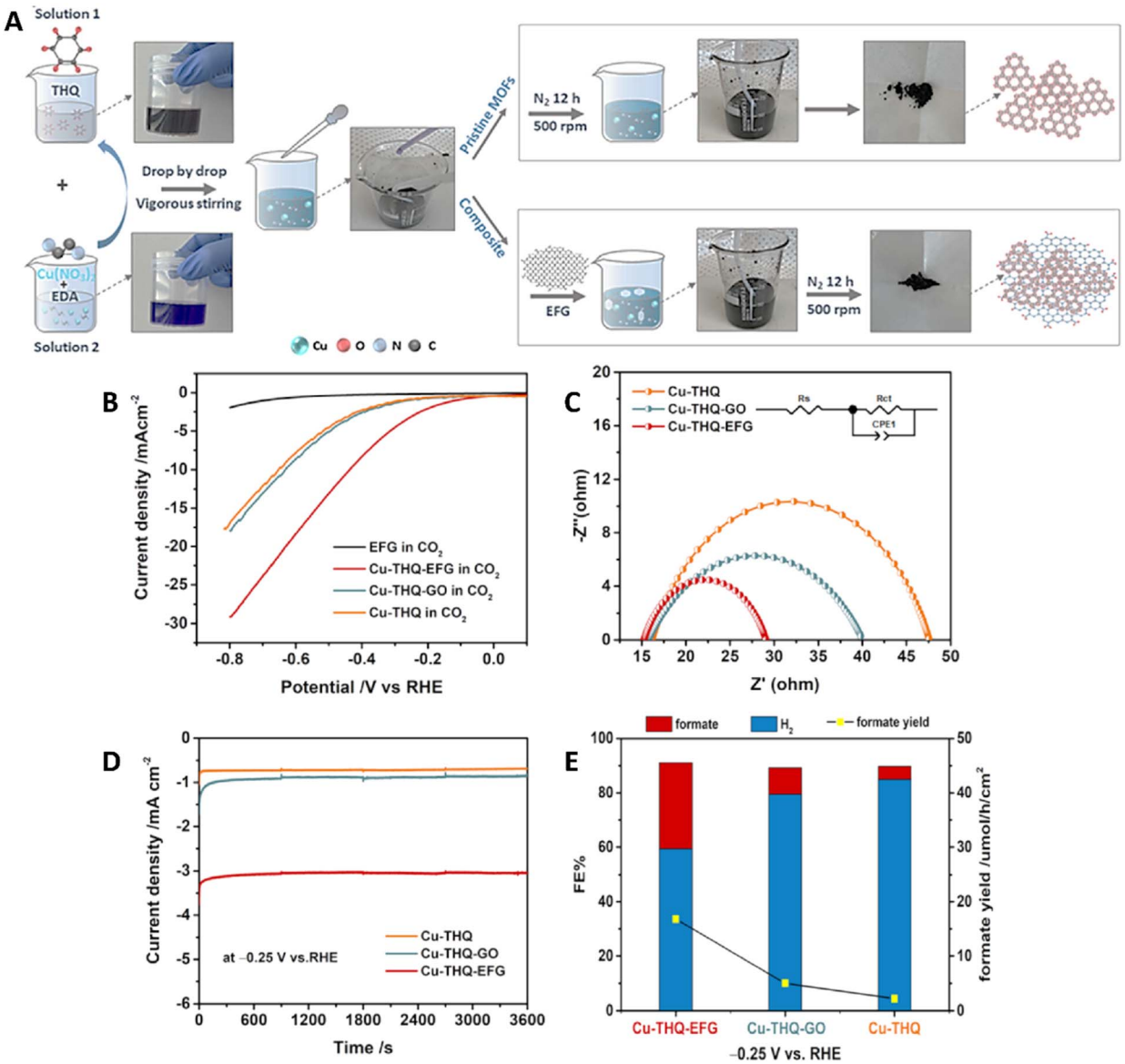

Fig. 9 (A) The schematic of the preparation process of the pristine and modified MOF (Cu-THQ MOF and Cu-THQ-EFG composite). (B) LSV curves, (C) EIS data, (D) current density, and (E) faradaic efficiency for Cu-THQ, Cu-THQ-GO and Cu-THQ-EFG. Reprinted with permission from ref. 154 under the terms and conditions of the Creative Commons Attribution (CC BY) license. Copyright 2022, MDPI.

© 2026 The Author(s). Published by the Royal Society of Chemistry

Open Access Article. Published on 23 February 2026. Downloaded on 4/9/2026 12:13:42 AM.
This article is licensed under a Creative Commons Attribution-NonCommercial 3.0 Unported Licence.

Similarly, conductive polymer-MOF composites were used to suppress competing hydrogen evolution reactions (HER). In this context, the incorporation of polyaniline into TcPcCo, a cobalt tetra-β-carboxyphthalocyanine, resulted in a faradaic efficiency of 95% within the potential range of −0.5 to −0.95 V. The presence of polyaniline reduced the activation energy required for forming the *COOH intermediate at the Co–N_4 site, which facilitated the CO_2 reduction while simultaneously suppressing the side reactions of hydrogen production and increasing the selectivity for CO production.[155]

The incorporation of metal nanoparticles into MOFs is a powerful method to improve catalytic activity. A composite electrocatalyst featuring silver nanoparticles (Ag NPs) embedded in thiol-functionalized, defect-engineered UiO-66 metal–organic frameworks (Ag@UiO-66-SH) was produced. Through coordination modulation, structural defects and thiol groups were introduced to serve as stable anchoring sites for Ag NPs, minimizing aggregation and maximizing active surface area. This catalyst demonstrated a faradaic efficiency of 74% for CO production at −1.1 V *versus* RHE and maintained a steady reduction current over 10 h, demonstrating exceptional catalytic stability and a mass-specific activity of 218 A g^{-1}. Complementary density functional theory calculations highlighted the improved CO_2 reduction reaction energetics of the modified material compared to its pristine form. These findings highlight the potential of metal NP-MOF hybrids with minimal metal loading as efficient and durable catalysts for selective CO_2 conversion to CO.[156]

To engineer an efficient electrocatalyst for CO_2 reduction, a molecular coordination strategy was employed to recombine bismuth and indium, forming Bi/In bimetallic MOFs. Upon calcination, these MOFs transformed into Bi/In bimetallic oxide nanoparticles, uniformly embedded within conductive carbon networks derived from decomposed organic linkers. This tailored architecture benefits from the synergistic interaction between Bi and In species, alongside a high surface area, optimized pore size distribution, and a defect-rich carbon matrix that offered superior electrical conductivity. Electrochemical evaluations demonstrated impressive formate production performance, with onset potentials as low as −0.45 V *vs.* RHE and faradaic efficiencies reaching up to 91% at −0.90 V. The catalyst also delivered a high partial current density of 22 mA cm^{-2} and a mass activity of 4900 mA mg^{-1}, maintaining over 91% efficiency over 48 h of continuous operation, which confirmed the stability of fabricated compound. Notably, the Bi–In oxide interfaces could modulate the binding energy of *OCHO intermediates, promoting high selectivity for formate while suppressing competitive hydrogen evolution. Coupled with enhanced CO_2 transport and electron mobility offered by the carbon matrix, the material demonstrated exceptional catalytic efficiency and long-term durability in CO_2 electroreduction applications.[157]

A promising approach to enhance MOF conductivity is designing two-dimensional structures. Two-dimensional nickel phthalocyanine (NiPc-NiO_4) MOF exhibited higher conductivity than its conventional counterparts. The nanosheet catalyst exhibited an onset potential of −0.50 V *vs.* RHE and achieved a peak faradaic efficiency of 98.4% for CO production at −0.80 V. At −0.90 V, the CO partial current density reached 34.5 mA cm^{-2}. The catalyst also demonstrated impressive long-term stability, maintaining over 90% faradaic efficiency across 8 h of continuous operation. Mechanistic insights supported by DFT calculations identified the Ni–N_4 coordination site within the phthalocyanine ring as the primary active center, which binds CO_2 and stabilizes the *COOH intermediate with a low energy barrier. The extended π-conjugated framework of the phthalocyanine backbone enabled rapid electron transfer from the electrode to the Ni sites, effectively lowering overpotential requirements.[127] Another effective strategy is converting MOFs into highly active and stable catalysts through thermal treatment methods (pyrolysis). In this process, the organic ligands decompose and form a porous carbon matrix in which metal or metal oxide nanoparticles are evenly distributed. The pyrolysis of Ni-ZIF-8 produced Ni–N_x–C structures that exhibited a faradaic efficiency of 98.2% for converting CO_2 to CO at a potential of −0.8 V *vs.* RHE and a current density of 200 mA cm^{-2}. DFT calculations showed that this transformation reduced the required activation energy of the formation of key intermediates during CO_2 production and thus improved the selectivity and overall catalytic activity.[158]

A novel hierarchical 1D/3D nitrogen-doped porous carbon (1D/3D NPC) was synthesized by carbonizing Zn-MOF-74 grown *in situ* on a melamine sponge, resulting in a conductive framework enriched with graphitic and pyridinic nitrogen sites. This architecture comprises one-dimensional carbon rods embedded within a three-dimensional porous scaffold, forming an interconnected network of macro-, meso-, and micropores that promote efficient CO_2 diffusion and uniform reactant distribution (Fig. 10). Spatial confinement within the 3D structure directed the growth of ultrathin carbon domains, which host positively charged carbon atoms adjacent to graphitic nitrogen key active sites for CO_2 electroreduction. Temperature-controlled carbonization enabled tunable nitrogen speciation and precise regulation of CO/H_2 output without altering the catalyst composition. The presence of nitrogen dopants and adjacent positively charged carbon sites lowered the activation energy required for CO_2 adsorption and formation of the key *COOH intermediate. Moreover, the conductive carbon network accelerated electron transfer to the active sites, enhancing overall catalytic efficiency. At −1.0 V *vs.* RHE, a current density of −60 mA cm^{-2} was recorded, with a faradaic efficiency of 75% for CO and 25% for H_2, resulting in a CO/H_2 ratio of 3.00. Long-term chronoamperometry at −0.8 V *vs.* RHE maintained impressive stability, with 95% current retention and 94% faradaic efficiency retention over 10 h. These results indicated that under optimized conditions, nearly two-thirds of electrons were efficiently directed toward CO formation, with the remainder contributing to hydrogen evolution.[159]

One of the advances that has attracted the attention of many researchers in recent years is the integration of computational tools like machine learning and density functional theory to accelerate the design and optimization of MOF catalysts. Machine learning models can easily predict the electrochemical behavior of MOFs based on key parameters such as pore size,

Open Access Article. Published on 23 February 2026. Downloaded on 4/9/2026 12:13:42 AM.
This article is licensed under a Creative Commons Attribution-NonCommercial 3.0 Unported Licence.

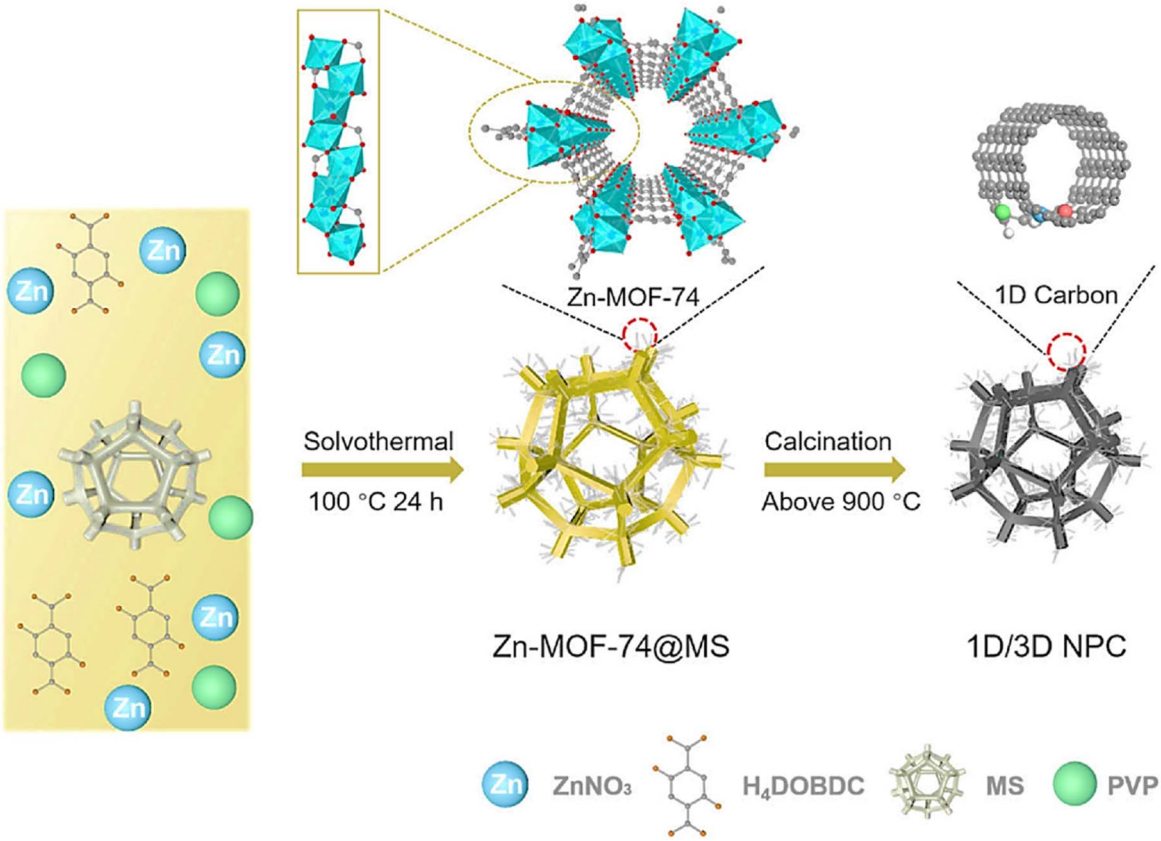

Fig. 10 Schematic illustration of the synthesis of 1D/3D NPC. Reprinted from ref. 159 under the terms of the Creative Commons CC BY license. Copyright 2023, Wiley.

central metal ions, and functional groups. This approach enables the identification and selection of promising MOF candidates for CO_2 reduction. For instance, researchers have integrated molecular dynamics (MD) simulations, active learning, and machine learning techniques to effectively predict the diffusion coefficients of molecules involved in CO_2 conversion in MOFs to facilitate the rational design of catalysts with enhanced performance.[160] Molecular dynamics simulations are employed to calculate mean squared displacements, enabling the estimation of diffusion coefficients through the Einstein relation. To encompass a wide range of pore structures and transport characteristics, an initial set of approximately 100 MOFs is simulated. Key structural and chemical descriptors such as pore limiting diameter, accessible surface area, void fraction, elemental composition metrics, and framework charge distributions are selected to characterize each MOF. Using these descriptors, an ensemble of random forest models predicts both the average diffusion rates and their associated uncertainties for MOFs not yet simulated. To strategically enhance the dataset, MOFs exhibiting either the highest prediction uncertainty or exceptionally high or low predicted diffusivity are selected for further MD simulations. This active learning (AL) strategy accelerates discovery by prioritizing informative samples. After three AL iterations (~400 simulations), prediction errors are reduced by a factor of approximately three compared to random sampling. The final machine learning model swiftly evaluates thousands of MOFs, pinpointing those with optimal diffusion profiles. By integrating diffusivity data with catalytic performance metrics, the framework identified MOFs that simultaneously maximize active site density and facilitated efficient molecular transport. Ultimately, this AL–ML approach dramatically curtails the need for costly MD simulations while enabling rapid, large-scale screening of MOFs. Accelerated identification of frameworks with finely tuned pore architectures and chemical properties for enhanced CO_2 conversion and reagent mobility.[161] Despite substantial progress, there are some challenges in scaling up MOFs for industrial applications. For instance, long-term stability of these catalysts is an issue, as MOF-based structures degrade during long-term operation and compromise their durability. Researchers have recently developed a scalable and efficient method for integrating MOFs into practical electrochemical systems for CO_2 reduction. They used the electrosynthesis method to synthesize MOF-based electrodes, which increased the electrical conductivity and improved the electrochemical performance. A recent study introduced an innovative method for growing the indium-based MOF, MFM-300(In), directly on metal foil using an applied electrical potential. This electrosynthesis approach dramatically improved the material's electronic conductivity by nearly tenfold compared to traditional

© 2026 The Author(s). Published by the Royal Society of Chemistry

Open Access Article. Published on 23 February 2026. Downloaded on 4/9/2026 12:13:42 AM. This article is licensed under a Creative Commons Attribution-NonCommercial 3.0 Unported Licence.

thermal synthesis thanks to two key structural changes. Electrochemical deposition created coordinated acetate vacancies and additional In^{3+} centers, which acted as promising sites for charge carriers. Simultaneously, the formation of smaller and more uniform octahedra shortened electron transport paths and increased exposure of defect-rich surfaces, effectively lowering bulk resistance. These enhancements enabled the electrosynthesized electrode to deliver a high current density of 46.1 mA cm^{-2} at −2.15 V *vs.* Ag/Ag^+ and a faradaic efficiency of 99.1% for formic acid production over a 2 h duration.[162]

Impressively, the device maintained stable performance over time, with only minimal overpotential drift; after 10 h, the current density remained strong at 44.8 mA cm^{-2} and faradaic efficiency held at 98.5%, far outperforming the thermally synthesized version, which dropped below 8 mA cm^{-2} and ~70% efficiency. Ultimately, the enhanced conductivity not only improved charge transport and lowered operational overpotentials, but also reduced heat generation and protected against bond cleavage, underscoring the impressive stability and efficiency of this electrosynthesized framework.[163] A recent study demonstrated that targeted molecular design combined with intelligent electrode engineering can effectively reduce the common degradation issues associated with MOF-based CO_2 reduction catalysts. Here, the Bi-BTC-D MOF featured a robust topology, where Bi^{3+} centers were securely connected to tricarboxylate ligands through strong Bi–O bonds. When tested under continuous electrolysis at −0.86 V *versus* RHE, the catalyst maintained a formate faradaic efficiency above 90% for 12 h, with effectively no drop in current density. Supporting this performance, DFT calculations indicated that undercoordinated Bi sites facilitate CO_2 activation by lowering the energy barrier, while maintaining thermodynamic stability during operation. Importantly, these active sites enhanced catalytic behavior without significantly disrupting the overall Bi–O coordination network, ensuring long-term performance and resilience.[164]

Traditional MOFs used for CO_2 electroreduction often face challenges such as limited gas uptake and high activation barriers at their active sites. To overcome these limitations, researchers have developed a honeycomb-like heterostructure by using a porous MOF core as a template. This architecture significantly boosted CO_2 adsorption capacity and, according to DFT, helped stabilize the *COOH intermediate while lowering its formation energy. These features accelerated the rate-limiting step in CO_2-to-CH_4 conversion. The study revealed that bulk MOF crystals tend to conceal numerous catalytic centers within their framework, limiting overall activity. To unlock these hidden sites, an ultrathin covalent organic framework (COF) shell was grown directly onto the MOF surface. The COF coating introduced a rich network of accessible active sites, with honeycomb pores extending throughout the entire particle ensuring that even interior surfaces actively contribute to catalysis. Moreover, the COF layer prevented MOF degradation during electrolysis, preserving site availability and structural integrity. This design resulted in a much higher catalytic site density than either material could achieve alone. Poor conductivity and sluggish mass transport typically reduced current output in MOF-based electrodes. The honeycomb heterostructure directly addressed this by forming continuous pathways for rapid electrolyte and CO_2 diffusion. It also established tight MOF–COF interfaces that significantly reduce charge-transfer resistance measured as low as ~3.3 Ω and elevated the current density to −398 mA cm^{-2} at −1.0 V. Conventional MOFs often struggle to distinguish between CO_2 reduction and hydrogen evolution, but MCH-3's synergistic MOF@COF design tips the balance in favor of CO_2 conversion. This structure improved CO_2 adsorption while suppressing local proton concentration, leading to a CH_4 faradaic efficiency of 76.7% a notable improvement over non-honeycomb analogs (≤47.7%) and physical mixtures (≤38.0%). Finally, long-term performance is often hindered by MOF collapse, metal ion leaching, and binder failure. The rigid COF shell mechanically reinforced the MOF crystals, shielding them from shear forces generated by gas bubbles. As a result, the electrode maintains more than 65% CH_4 faradaic efficiency and a current density of −359 mA cm^{-2} over 90 min of operation, with no detectable loss of crystallinity (Fig. 11).[165]

It is expected that with ongoing innovation and the integration of advanced synthesis methods, MOFs will evolve into increasingly efficient, scalable, and commercially viable electrocatalysts for practical CO_2 reduction applications.

4 Combination of MXenes and MOFs

The integration of two-dimensional (2D) materials is gaining advancement as a promising strategy for constructing multifunctional composites with improved properties. Among various 2D materials, MXenes exhibit remarkable features such as high surface area, redox activity, electrical conductivity, and tunable interlayer spacing. However, their practical application is often hindered by issues such as aggregation of sheets and oxidative degradation, which diminish their surface accessibility and overall stability (Table 2). Another type of 2D materials is MOFs that exhibit remarkable characteristics such as high porosity, adjustable pore dimensions, and significant redox capabilities, making them attractive candidates for applications in sensing, electrocatalysis, energy storage, water purification, and biomedicine (Table 2).

Nonetheless, their limited electrical conductivity and moderate stability restrict their broader use. The hybridization of MXenes with MOFs has emerged as a synergistic approach to overcome these individual limitations. By inserting MOF structures between MXene layers, aggregation is reduced and stability is enhanced, while also introducing additional porosity and redox-active sites. This complementary interaction not only preserves but also enhances the desirable attributes of both components, leading to MXene@MOF composites with superior physicochemical, mechanical, and electrochemical performance. The ability to fine-tune the composition and architecture of these hybrid systems opens new avenues for designing smart materials tailored to next-generation applications.[173–176] Beyond structural complementarity, the enhanced CO_2 electroreduction performance of MXene–MOF composites arise from well-defined mechanistic synergy

Open Access Article. Published on 23 February 2026. Downloaded on 4/9/2026 12:13:42 AM.
This article is licensed under a Creative Commons Attribution-NonCommercial 3.0 Unported Licence.

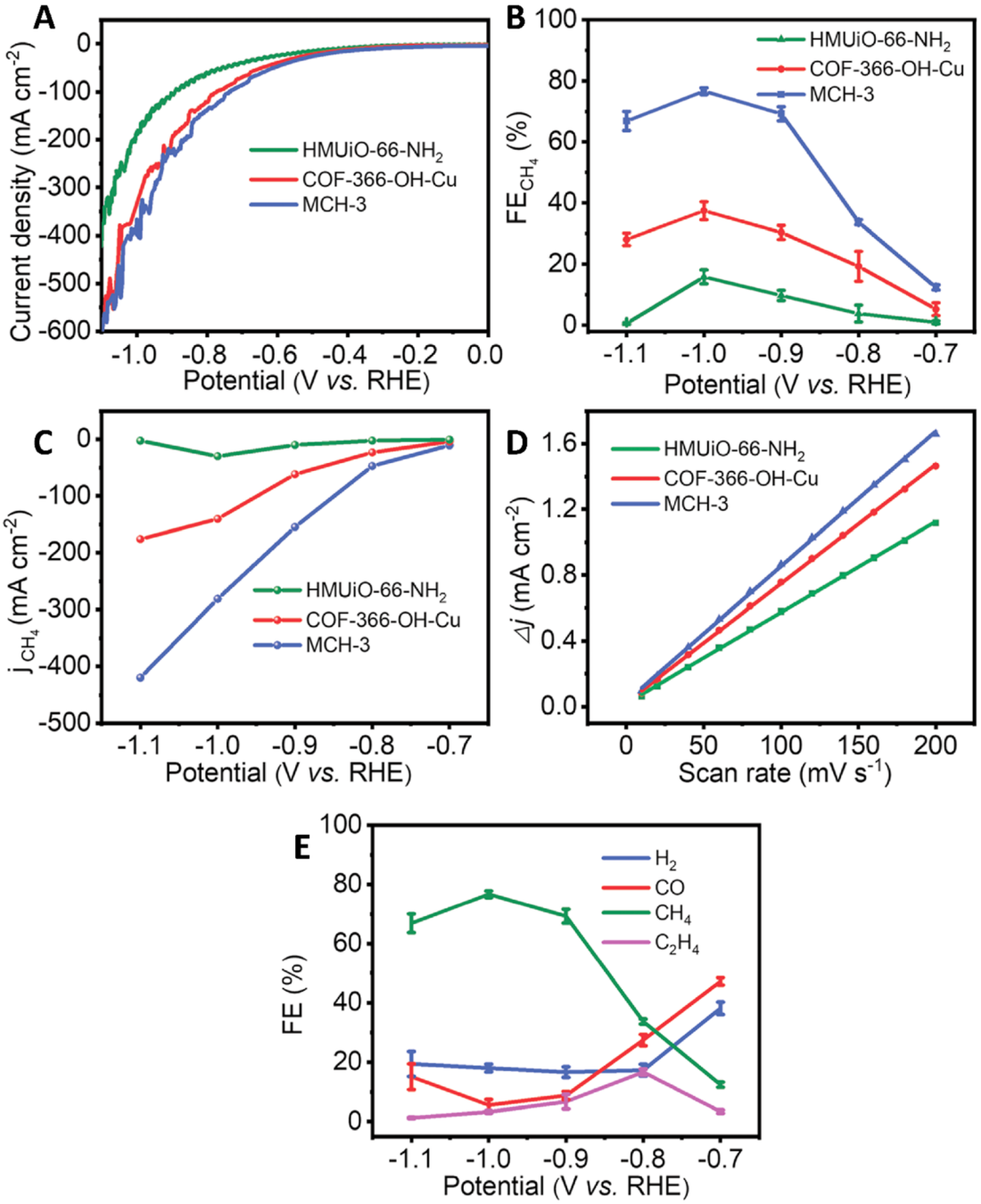

Fig. 11 (A) Linear scan voltammetry curves of HMUiO-66-NH_2, COF-366-OH-Cu, and MCH-3. (B) Faradaic efficiency CH_4 calculated over potential range from −0.7 to −1.1 V. (C) Partial CH 4 current density. (D) Capacitive current at 0.05 V as a function of scan rate for HMUiO-66-NH_2, COF-366-OH-Cu, and MCH-3. (E) Faradaic efficiencies of MCH-3 at different applied potentials. Reprinted with permission from ref. 165. Copyright 2022, Wiley.

between the two components. In these hybrid systems, MXenes primarily act as highly conductive electron transport platforms, enabling rapid charge transfer to catalytically active sites, while their surface terminations (–O, –OH, and –F) facilitate CO_2 adsorption and contribute to the stabilization of key reaction intermediates through electrostatic interactions and hydrogen bonding.[31] At the same time, MOFs provide atomically dispersed metal nodes with tailored coordination environments that function as the principal catalytic centers, where CO_2 activation and product selectivity are governed by metal–ligand interactions.[177] Importantly, the formation of MXene–MOF interfaces generate unique interfacial active sites characterized by electronic coupling and charge redistribution, which modulate the electronic structure of MOF metal centers and lower the energy barriers for intermediate formation. Such interfacial effects play a crucial role in stabilizing critical CO_2

© 2026 The Author(s). Published by the Royal Society of Chemistry

Open Access Article. Published on 23 February 2026. Downloaded on 4/9/2026 12:13:42 AM. This article is licensed under a Creative Commons Attribution-NonCommercial 3.0 Unported Licence.

Table 2 Advantages and disadvantages of application of MOFs and MXenes-based materials for CO_2RR

Material	Advantages	Disadvantages
MOFs	Exceptionally high surface area and tunable porosity for efficient CO_2 adsorption and enhanced mass transport[98,166]	Low intrinsic electrical conductivity of many pristine MOFs, which impedes charge transfer and requires composite engineering[98,167]
	Unprecedented chemical and structural tunability *via* rational selection of metal nodes and organic linkers to tailor activity, selectivity, and stability[166]	Limited long-term electrochemical stability under operating conditions, particularly in acidic or alkaline media, leading to framework degradation[167,168]
	Atomically uniform and high-density dispersion of catalytic sites (*e.g.*, single metal atoms or clusters) within the ordered framework[98,166]	Mass transfer limitations within predominantly microporous structures, necessitating the design of hierarchical porosity for efficient diffusion[167]
	Precise engineering of the local catalytic environment (*e.g.*, secondary coordination spheres) to control intermediate binding and direct reaction pathways[166]	Insufficient chemical stability for some MOFs in aqueous or reactive electrochemical environments, risking dissolution or ligand displacement[167,168]
	Versatile precursor functionality for conversion into MOF-derived materials (*e.g.*, doped carbons, alloys) that retain favorable porosity while gaining enhanced conductivity and stability[98,167]	Scalability and cost challenges associated with the synthesis of advanced, stable MOFs, limiting their practical, large-scale application[166,167]
MXenes	MXenes exhibit metallic conductivity that facilitates rapid electron transfer during multi-electron CO_2RR steps, which can improve catalytic activity[31]	MXenes can restack or degrade under electrochemical conditions, reducing active surface area and long-term performance[169]
	MXene edges, defects, and terminations provide multiple active sites for CO_2 adsorption and reduction[31]	In some MXenes, the density of inherently active sites may be insufficient without dopants, composites, or heterostructures[170]
	The layered structure provides a high surface area favorable for catalyst dispersion[31]	Conventional etching uses HF or similar corrosive reagents, posing safety, reproducibility, and scalability challenges for large-scale catalyst production[169]
	Surface functional groups (–O, –OH, –F, –Cl) can be engineered to modulate CO_2 adsorption and intermediate binding, offering pathways to tailor selectivity[32]	Achieving precise and stable control of surface terminations during synthesis is difficult, leading to variability in performance and challenges in rational catalyst design[169]
	MXenes can support single-atom catalysts or be integrated into hybrid materials to potentially enhance catalytic performance[171]	MXenes are prone to oxidation in air or under electrochemical conditions, degrading performance over time[169]
	MXenes can effectively adsorb and activate CO_2, with some showing favorable energetics for CO_2RR pathways[172]	

reduction intermediates, including $*CO_2^-$, *COOH, and OCHO species, thereby enhancing reaction kinetics, suppressing competing hydrogen evolution, and enabling improved selectivity toward desired carbon-based products. These mechanistic aspects underscore that the superior performance of MXene@MOF composites originates not from a simple additive effect but from cooperative interfacial catalysis, which will be discussed in detail in the following sections.[32,178] Different methods have been introduced for the fabrication of MXene@MOF composites some of them are mentioned in Table 3.

As mentioned earlier, lowering atmospheric CO_2 levels has become a critical global priority, as CO_2 is a major driver of climate change and related environmental issues. To address this challenge, different methods have been developed and studied to reduce the microenvironmental level of CO_2.[30,192,193] These CO_2 molecules could be considered as a renewable source for producing chemical compounds using photocatalytic or electrocatalytic reactions. In other words, these clean fuels could act as the alternatives of oil source in producing valuable materials. Therefore, different types of catalytic methods have been introduced to capture and convert CO_2 molecules, even at low amounts.[30,180,194]

In another study, MXene–MOF hybrid catalysts was produced through the synthesis of a MXene/ZIF-8 composite, in which ZIF-8 nanocrystals were uniformly grown on MXene nanosheets *via* a layer-by-layer assembly strategy. This architecture effectively prevented MXene restacking while enhancing the electrical conductivity of the MOF component and increasing the accessibility of catalytically active sites. Electrochemical evaluation revealed that the composite exhibited markedly improved performance compared to its individual constituents, demonstrating high capacitance and excellent cycling stability when employed as a supercapacitor electrode. More importantly, in electrocatalytic CO_2 reduction, the MXene/

Open Access Article. Published on 23 February 2026. Downloaded on 4/9/2026 12:13:42 AM.
This article is licensed under a Creative Commons Attribution-NonCommercial 3.0 Unported Licence.

Table 3 Different methods that were used for production of MXene@MOF composites, their advantages and disadvantages

Synthesis method	Brief description	Sample	Advantages	Disadvantages	Ref.
In situ synthetic approach	MOF grows directly on MXene sheets *via* interdiffusion of metal salts and organic linkers in a solvent medium	CoBDC/$Ti_3C_2T_x$	Preserves structures of both components Improved structural and hydrothermal stability Strong MOF-MXene interactions Enhanced catalytic activity (*e.g.*, OER)	May involve long synthesis times or hydrothermal conditions Sensitive to solvent composition and synthesis conditions	179–181
Direct mixing method	Simple physical mixing of pre-synthesized MOF and MXene, followed by mild processing	PCN-224 MOF/$Ti_3C_2T_x$	Scalable and easy to perform Mild conditions Preserves individual MOF and MXene properties Flexible substrate compatibility	Weak interfacial bonding (van der Waals, H-bonding) Random distribution of components Limited structural integration	182–184
MOF-derived composites	MOF@MXene hybrids are thermally treated to derive new materials	CoO_x-NC/TiO_2C	Produces functional materials with high surface area, redox activity Hierarchical porous structures Applicable for electrocatalysis and energy storage Tunable compositions and morphologies	High-temperature treatment may degrade structure Possible oxidation of MXene Complex synthesis routes	185 and 186
Electrostatic assembly strategy	Positively charged are assembled with negatively charged MXene nanosheets *via* electrostatic interactions, then thermally annealed	Co-ZIF-9/Ti_3C_2	Enables formation of hollow and porous structures Maintains charge balance for uniform coating Suitable for building composite films and nanostructures	Requires careful control of surface charges (zeta potential) Possible agglomeration during drying or annealing	187 and 188
Electrochemical synthesis	MOF films or layers are electrodeposited directly onto MXene substrates using an electrochemical workstation. This involves using the MXene-covered electrode as working electrode while metal ions and organic linkers deposit *in situ* under controlled potential conditions	MXene-ZIF-8 membranes MXene-Ni-Co@NiCo-MOF/NF	Precise control over layer thickness and morphology Mild, rapid synthesis conditions Real-time monitoring and scalability Strong adhesion between MOF and MXene Minimizes restacking and oxidation of MXene Produces conductive composite electrodes suited for capacitors or electrocatalysis	Requires electrochemical setup and optimization of deposition parameters Limited to conductive substrates and electrode applications May form thin or uneven coatings if conditions are not optimized Not yet widely reported specifically for MOF-on-MXene combinations	189–191

© 2026 The Author(s). Published by the Royal Society of Chemistry

Open Access Article. Published on 23 February 2026. Downloaded on 4/9/2026 12:13:42 AM. This article is licensed under a Creative Commons Attribution-NonCommercial 3.0 Unported Licence.

ZIF-8 hybrid achieved a high faradaic efficiency for syngas (CO + H_2) production at significantly lower overpotentials than the pristine MOF. The enhanced CO_2RR activity was attributed to synergistic effects arising from the conductive MXene framework, which facilitated rapid electron transfer, and the porous ZIF-8 structure, which provided abundant metal–ligand active sites and promoted CO_2 adsorption. This study highlights how interfacial coupling in MXene–MOF composites can effectively regulate charge transport and reaction kinetics, thereby improving catalytic efficiency and selectivity.[195]

In another study, in-based porphyrin frameworks (In-TCPP) were produced on the surface of $Ti_3C_2T_x$ MXenes. Presence of porphyrin in the structure of this composite could building blocks for making MOF-based electrocatalysts with large π-conjugated systems that help in stabilizing the structure of MOF and allowing electrons to move more easily during reactions. They also had good redox properties, which support reactions involving the transfer of multiple electrons, especially useful in CO_2 reduction into the HCOOH. Additionally, the rigid structure of porphyrins led to creating larger pores in the material, which improved the exposure of active sites and enhanced catalytic performance. Besides, the interaction between In-TCPP and MXene led to a significant charge redistribution, which altered the electronic structure of the indium (In) sites and improved the adsorption of CO_2 molecules, that further enhancing the reaction process. The fabricated composite showed Faraday efficiency of about 94% for $HCOO^-$ and high stability during 15 h electrolysis.[196]

5 Challenges and limitations

Although MXenes and MOFs have shown great promise as catalysts and composite materials for CO_2 electroreduction, several critical challenges limit their practical implementation. One major challenge is the inherently low electrical conductivity of MOFs, which restricts efficient charge transfer during catalysis.[197,198] This is partly overcome by integrating MXenes, which possess excellent electrical conductivity, but synthesis of stable and well-integrated composites remains complex.[19,26,33] Both materials face stability issues under harsh electrochemical conditions: MXenes are prone to surface oxidation that degrades the metallic layers essential for conductivity,[199–201] while MOFs can suffer from structural degradation and instability in aqueous and electrochemical environments.[202] Additionally, controlling the selectivity of CO_2 reduction to desirable products remains difficult due to competing side reactions, including hydrogen evolution, limiting efficiency and product yield.[203]

Stability and durability are among the most critical challenges for MXene/MOF catalysts in electrochemical CO_2 reduction. MXenes tend to undergo irreversible oxidation, which degrades their metallic carbide or nitride layers, leading to reduced electrical conductivity and catalytic performance over time. This oxidation diminishes electron transfer efficiency, eventually causing catalyst deactivation.[199–201,204] On the MOF side, many frameworks suffer from chemical instability under the harsh reductive or acidic conditions typical in CO_2 electroreduction, leading to collapse or dissolution of the MOF structure. The repeated cycling and prolonged operation can exacerbate these effects.[22,205] Researchers are actively exploring surface modifications, protective coatings, and heterostructure engineering (*e.g.*, Schottky junctions with MXenes) to improve stability and prolong the catalytic lifetimes of these materials.

Scalability of composite synthesis remains a significant hurdle. Achieving strong and stable coupling between MXenes and MOFs is critical for efficient charge transfer and catalytic synergy, but controlling these nanostructures reproducibly at scale is nontrivial. Conventional MXene synthesis involves harsh etching processes, typically with fluoride-containing chemicals, which pose challenges for large-scale, cost-effective, and environmentally safe production.[206,207] Similarly, MOFs often require long reaction times, high temperatures, specialized equipment, and large volumes of organic solvents to achieve high crystallinity, porosity, and chemical stability. While emerging techniques such as microwave-assisted, spray-drying, mechanochemical, and microfluidic synthesis enable gram-scale production.[208,209] Reproducible industrial-scale synthesis (kilogram or larger) remains largely untested. Furthermore, integrating MXene/MOF composites into durable electrodes and electrolyzer systems capable of continuous operation is still in early stages, with mass transport, catalyst loading, and electrode architecture posing additional obstacles.

From an industrial translation perspective, the aforementioned challenges become significantly more severe under commercially relevant operating conditions. Industrial CO_2 electrolysis typically requires high current densities (>200–500 mA cm^{-2}), continuous operation over hundreds to thousands of hours, and integration into gas diffusion electrodes (GDEs) or membrane electrode assemblies (MEAs). Under such conditions, the degradation mechanisms of MXene/MOF catalysts, including MXene oxidation, MOF framework collapse, catalyst delamination, and loss of active surface area, are markedly accelerated due to intensified local pH gradients, Joule heating, gas bubble accumulation, and mechanical stresses. Notably, most reported MXene- and MOF-based CO_2 reduction studies evaluate stability over relatively short durations (tens of hours) and at low current densities, which do not adequately reflect industrial durability requirements. Furthermore, stabilization strategies effective at the laboratory scale, such as surface passivation layers, complex heterostructure engineering, or multi-step synthesis routes, may substantially increase material complexity and production costs, posing additional barriers to large-scale manufacturing and commercialization. Therefore, bridging the gap between laboratory demonstrations and industrial CO_2 electrolysis necessitates the development of intrinsically robust catalyst architectures, scalable electrode fabrication strategies, and standardized durability testing protocols under industrially relevant conditions.[63,210–214]

Economic factors play a crucial role in the deployment of MXenes and MOFs for electrochemical CO_2 reduction. The cost of raw materials, complex synthesis routes, and post-processing steps make these materials expensive when compared to traditional catalysts. Strategies to improve economic viability include using cheaper metal nodes or organic linkers in MOFs,

Open Access Article. Published on 23 February 2026. Downloaded on 4/9/2026 12:13:42 AM. This article is licensed under a Creative Commons Attribution-NonCommercial 3.0 Unported Licence.

developing greener etching processes for MXenes, and adopting scalable continuous-flow synthesis methods. A holistic evaluation of industrial feasibility should consider not only catalyst costs but also electrodes, device fabrication, energy input, and product value to ensure competitiveness with existing CO_2 capture and conversion technologies. Additionally, the long-term durability issues could lead to frequent catalyst replacement, increasing operational costs. To be commercially viable, these catalysts must not only exhibit high activity and selectivity but also offer low production costs and robust lifetimes. Developing cost-effective synthesis methods, such as greener etching processes for MXenes, and using cheaper metal centers or organic linkers in MOFs are important research directions. Besides, economic assessments must consider the entire system cost, including catalyst, electrodes, and device manufacturing, alongside energy input and product value, to ensure the technology can compete with existing CO_2 capture and conversion methods.[19,24,25,215]

Beyond the major challenges of stability, scalability, and economics already discussed, several other notable challenges exist in the electrochemical reduction of CO_2 using MXenes and MOFs. One key issue is the intrinsic poor selectivity and controlling the product distribution during CO_2 reduction. The complex multi-electron and proton transfer pathways can lead to a variety of reduction products, including hydrogen from competing hydrogen evolution reaction (HER), which lowers the efficiency of CO_2 conversion and complicates the separation and use of products. Precise tuning of the surface chemistry and electronic structure of MXenes and MOFs to selectively stabilize intermediates for desired products remains difficult. Notably, the inherent metallic nature of pristine MXenes makes them unable to absorb solar energy efficiently in photocatalytic CO_2 reduction, requiring modifications to induce semiconducting behavior or careful composite design.[16,216] The complexity of balancing electronic properties, stability, and catalytic activity in these hybrid materials is a continuing research challenge. Lastly, device integration challenges remain, including mass transport limitations and catalyst stability under realistic operating conditions of electrolyzed or photoelectrochemical cells. Efficient transport of CO_2 to active sites and removal of products, while maintaining catalyst integrity under prolonged cycling, are necessary for real-world applications but still require significant engineering advances.

6 Future perspectives

The synergistic integration of MXenes, especially Ti_3C_2, with MOFs enhances electrical conductivity, catalytic activity, and stability, opening new frontiers for highly efficient CO_2 conversion. Research is increasingly focusing on engineering binary and ternary composites and heterojunctions that optimize charge separation and transfer, thereby improving selectivity towards valuable products like CO and formic acid. Additionally, an important direction for future studies is overcoming current stability and durability issues by modifying surface chemistries and developing protective coatings or heterostructures. MXenes are prone to oxidation, while MOFs face structural degradation in harsh electrochemical environments. Future research will likely leverage advanced surface functionalization and design strategies to prolong catalyst lifetime while maintaining activity. Utilizing machine learning and high-throughput computational screening to identify optimal MXene/MOF combinations with enhanced robustness and catalytic efficiency is a growing trend anticipated to accelerate discoveries and reduce experimental trial-and-error.

Scaling up synthesis methods for producing high-quality MXene/MOF composites at industrially relevant scales is another critical future challenge. Current MXene production involves harsh chemical etching processes that pose safety, environmental, and cost issues. Emerging scalable synthesis approaches, such as continuous flow processes and greener chemistries, alongside integration with existing industrial platforms, are expected to drive wider application. Similarly, developing cost-effective, reproducible, and scalable MOF production will be crucial for commercial viability. Progress in scalable fabrication will be paired with advances in electrode and electrolyzed system engineering to realize durable, high-performance devices for real-world CO_2 conversion.

From an application standpoint, integrating MXene/MOF-based catalysts into flexible, modular, and renewable-powered electrolyzed systems presents a path toward sustainable carbon-neutral fuel synthesis. Future systems may combine CO_2 reduction with other renewable energy conversion and storage technologies. Advances in reactor design that improve mass transport, enhance CO_2 accessibility, and facilitate product separation will further enhance process efficiency. Such integrated, well-engineered platforms can enable decentralized, small-to-medium scale CO_2 conversion units suitable for various industrial and environmental settings, greatly expanding impact. Notably, economic and environmental considerations will drive future research to enhance the overall sustainability of these technologies. Efforts to reduce raw material costs, extend catalyst lifetimes, and improve energy efficiency will be essential to compete with conventional processes. Research will also focus on minimizing environmental impact through green synthesis methods and lifecycle assessments.

7 Conclusion

MXenes and MOFs have emerged as highly promising materials for advancing the electrochemical reduction of CO_2, owing to their complementary properties. MOFs offer extraordinary porosity, tunable chemistry, and abundant active sites, while MXenes provide excellent electrical conductivity and surface functionalization that facilitate rapid charge transfer. The integration of these materials into composites has demonstrated synergistic effects, leading to improved catalytic activity, selectivity, and stability for CO_2 reduction to valuable products such as CO and formic acid. Recent breakthroughs in designing heterojunctions and hybrid structures underscore the potential of MXene/MOF systems to address performance limitations that have traditionally hindered electrochemical CO_2 conversion.

© 2026 The Author(s). Published by the Royal Society of Chemistry

Open Access Article. Published on 23 February 2026. Downloaded on 4/9/2026 12:13:42 AM. This article is licensed under a Creative Commons Attribution-NonCommercial 3.0 Unported Licence.

Despite these encouraging developments, significant challenges remain to be solved before MXene/MOF-based catalysts can be broadly applied at an industrial scale. Stability and durability under harsh electrochemical conditions, particularly MXenes' susceptibility to oxidation and MOFs' chemical degradation, continue to limit long-term usability. The complexity and costs associated with synthesizing high-quality MXene/MOF composites, alongside concerns around scalability, mass transport limitations, and electrode integration, present further obstacles. Moreover, economic considerations including material costs and catalyst lifetimes must be carefully balanced against activity and selectivity enhancements to achieve commercial viability. Addressing these multifaceted challenges requires a concerted effort across materials engineering, green chemistry, and device fabrication.

The future of MXenes and MOFs in CO_2 electroreduction is very promising, fueled by advances in material design, computational modeling, and synthesis techniques. Emerging strategies such as advanced surface functionalization, protective coatings, and machine learning-guided screening are expected to yield catalysts with enhanced stability and tailored catalytic properties. Development of scalable and environmentally benign production methods for MXene/MOF composites will be essential to facilitate their practical deployment. Simultaneously, integrating these catalysts into flexible, efficient electrolyzer systems powered by renewable energy could pave the way for decentralized and sustainable CO_2 conversion technologies that contribute meaningfully to carbon neutrality goals. The dynamic interaction between fundamental materials innovation and applied engineering will dictate the successful translation of MXene/MOF catalysts from laboratory research to real-world applications. With additional exploration, these materials hold great promise for enabling efficient, selective, and durable electrochemical CO_2 reduction, helping to transform greenhouse gases into valuable fuels and chemicals. This progress aligns strongly with global efforts toward mitigating climate change and fostering a sustainable energy future.

Author contributions

Elham Momtaz: writing – review & editing; Masoomeh Amoozadeh: writing – review & editing; Atefeh Zarepour: writing – review & editing; Arezoo Khosravi: visualization, writing – review & editing; Ali Zarrabi: supervision, writing – review & editing; Siavash Iravani: supervision, conceptualization, writing – review & editing. All authors reviewed the manuscript.

Conflicts of interest

The authors declare no conflict of interest.

Data availability

No primary research results, software or code have been included, and no new data were generated or analyzed as part of this review.

References

1 S. Varhade, A. Guruji, C. Singh, G. Cicero, M. García-Melchor, J. Helsen and D. Pant, *ChemElectroChem*, 2025, **12**, e202400512.
2 Z. M. Ghazi, D. Ewis, H. Qiblawey and M. H. El-Naas, *Carbon Capture Sci. Technol.*, 2024, **13**, 100308.
3 S. Dell'Aversano, C. Villante, K. Gallucci, G. Vanga and A. Di Giuliano, *Energies*, 2024, **17**, 3995.
4 E. Hanson, C. Nwakile and V. O. Hammed, *Results Surf. Interfaces*, 2025, **18**, 100381.
5 Q. Li, X. You, J. Wu and Z. Tang, *Adv. Funct. Mater.*, 2025, **35**, e08825.
6 S. Zhong, B. Chen, D. Tang, Q. Yang, W. Weng and X. F. Lu, *Chem. Commun.*, 2025, **61**, 12010–12013.
7 B. Belsa, L. Xia and F. P. García de Arquer, *ACS Energy Lett.*, 2024, **9**, 4293–4305.
8 D. Segets, C. Andronescu and U. P. Apfel, *Nat. Commun.*, 2023, **14**, 7950.
9 Y. A. Alli, A. Bamisaye, M. O. Bamidele, N. O. Etafo, S. Chkirida, A. Lawal, V. O. Hammed, A. S. Akinfenwa, E. Hanson, C. Nwakile, K. O. Kazeem, R. J. Ayanwunmi, A. S. Ige, J. R. Torres and H. A. Nageim, *Results Surf. Interfaces*, 2024, **17**, 100321.
10 F. Yu, K. Deng, M. Du, W. Wang, F. Liu and D. Liang, *Carbon Capture Sci. Technol.*, 2023, **6**, 100081.
11 O. U. Patil and S. Park, *Chem. Commun.*, 2025, **61**, 9531–9542.
12 L. Liu, H. Akhoundzadeh, M. Li and H. Huang, *Small Methods*, 2023, **7**, 2300482.
13 H. Wu, A. Singh-Morgan, K. Qi, Z. Zeng, V. Mougel and D. Voiry, *ACS Catal.*, 2023, **13**, 5375–5396.
14 F. Liu, J. Deng, B. Su, K.-S. Peng, K. Liu, X. Lin, S.-F. Hung, X. Chen, X. F. Lu and Y. Fang, *ACS Catal.*, 2025, **15**, 1018–1026.
15 Y. Zhao, Z. Pei, X. F. Lu, D. Luan, X. Wang and X. W. Lou, *Chem Catal.*, 2022, **2**, 1480–1493.
16 B. Tahir, A. Alraeesi and M. Tahir, *Front. Chem.*, 2024, **12**, 1448700.
17 T. Amrillah, A. R. Supandi, V. Puspasari, A. Hermawan and Z. W. Seh, *Trans. Tianjin Univ.*, 2022, **28**, 307–322.
18 U. Aizaz, I. U. Hassan and S. A. Onaizi, *Renew. Sustain. Energy Rev.*, 2025, **214**, 115524.
19 A. Aldhaher, N. Rabiee and S. Iravani, *Hybrid Adv.*, 2024, **5**, 100131.
20 S. I. Basha, S. S. Shah, A. Helal, M. Abdul Aziz and D. Y. Yoo, *Case Stud. Constr. Mater.*, 2024, **21**, e03586.
21 J. Zhu, X. F. Lu, D. Luan and X. W. Lou, *Angew. Chem., Int. Ed.*, 2024, **63**, e202408846.
22 J. M. Huang, X. D. Zhang, J. Y. Huang, D. S. Zheng, M. Xu and Z. Y. Gu, *Coord. Chem. Rev.*, 2023, **494**, 215333.
23 Y. Gogotsi and B. Anasori, *ACS Nano*, 2019, **13**, 8491–8494.
24 Y. Chen, Y. Shi, G. Song, B. Yang and H. Pang, *Next Mater.*, 2025, **6**, 100323.
25 S. Feng, S. Wen, R. Wang, X. Yang, X. Yuan, Y. Liu, J. Ma and Z. Li, *Nanomaterials*, 2025, **15**, 841.

Open Access Article. Published on 23 February 2026. Downloaded on 4/9/2026 12:13:42 AM. This article is licensed under a Creative Commons Attribution-NonCommercial 3.0 Unported Licence.

26 I. Hussain, A. A. Mahmud, R. Amna, A. H. Pato, U. Sajjad, Z. Ajmal and K. Zhang, *Mater. Today*, 2025, **89**, 344–373.
27 J. Liu, C. Chen, K. Zhang and L. Zhang, *Chin. Chem. Lett.*, 2021, **32**, 649–659.
28 M. Jussambayev, K. Shakenov, S. Sultakhan, U. Zhantikeyev, K. Askaruly, K. Toshtay and S. Azat, *Carbon Trends*, 2025, **19**, 100471.
29 A. E. Mathew, S. Jose, A. M. Babu and A. Varghese, *Mater. Today Chem.*, 2024, **36**, 101927.
30 Y. Meng, F. Yue, S. Zhang, L. Zhang, C. Li, M. Shi, Y. Ma, M. Berrettoni, X. Zhang and H. Zhang, *Carbon Capture Sci. Technol.*, 2024, **13**, 100274.
31 S. A. Talas, P. D. Kolubah, R. Khairova, M. Alqahtani, S. I. El-Hout, F. M. Alissa, J. K. El-Demellawi, P. Castaño and H. O. Mohamed, *Mater. Horiz.*, 2025, **12**, 7648–7682.
32 B. Tahir, A. Alraeesi and M. Tahir, *Front. Chem.*, 2024, **12**, 1448700.
33 F. Zhang, Y. Qian, Z. Jin, Z. Fei, J. Zhang, H. Mao, D. J. Kang and H. Pang, *J. Energy Storage*, 2023, **72**, 108213.
34 X. Zhuang, S. Zhang, Y. Tang, F. Yu, Z. Li and H. Pang, *Coord. Chem. Rev.*, 2023, **490**, 215208.
35 M. Safarkhani, A. Aldhaher, E. C. Lima, M. Zargar, E. E. Jung, Y. S. Huh and N. Rabiee, *ACS Appl. Eng. Mater.*, 2023, **1**, 3080–3098.
36 C. Y. J. Lim, A. D. Handoko and Z. W. Seh, *Diamond Relat. Mater.*, 2022, **130**, 109461.
37 N. Farzizadeh, A. Zarepour, A. Khosravi, S. Iravani and A. Zarrabi, *Mater. Adv.*, 2025, **6**, 5807–5830.
38 S. Iravani, A. Zarepour, A. Khosravi, A. Zarrabi, E. N. Zare, R. S. Varma and P. Makvandi, *Mater. Adv.*, 2025, **6**, 5011–5029.
39 D. Khorsandi, J.-W. Yang, Z. Ülker, K. Bayraktaroğlu, A. Zarepour, S. Iravani and A. Khosravi, *Microchem. J.*, 2024, **197**, 109874.
40 Y. Zhong, H. Zhu, H. Zhang, X. Xie, L. Yang, B. Wang, Q. Fan, Z. Xie and Z. Le, *Green Chem.*, 2025, **27**, 5455–5463.
41 R. M. Ronchi, J. T. Arantes and S. F. Santos, *Ceram. Int.*, 2019, **45**, 18167–18188.
42 L. Meng, E. Tayyebi, K. S. Exner, F. Viñes and F. Illas, *ChemElectroChem*, 2024, **11**, e202300598.
43 H. Chen, A. D. Handoko, T. Wang, J. Qu, J. Xiao, X. Liu, D. Legut, Z. Wei Seh and Q. Zhang, *ChemSusChem*, 2020, **13**, 5690–5698.
44 M. H. Jameel, M. Arain, I. Hussain, M. B. Hanif, S. Atri, M. Z. H. Mayzan and H. Dai, *Nano Mater. Sci.*, 2024, **7**, 444–481.
45 P. O. Persson and J. Rosen, *Curr. Opin. Solid State Mater. Sci.*, 2019, **23**, 100774.
46 Z. Li, N. H. Attanayake, J. L. Blackburn and E. M. Miller, *Energy Environ. Sci.*, 2021, **14**, 6242–6286.
47 M. Amoozadeh, A. Zarepour, A. Khosravi, S. Iravani and A. Zarrabi, *FlatChem*, 2025, **51**, 100849.
48 X.-Q. Tan, W. Mo, X. Lin, J. Y. Loh, A. R. Mohamed and W.-J. Ong, *Nanoscale*, 2023, **15**, 6536–6562.
49 L. He, H. Zhuang, Q. Fan, P. Yu, S. Wang, Y. Pang, K. Chen and K. Liang, *Mater. Horiz.*, 2024, **11**, 4239–4255.
50 B. Ansori and Y. Gogotsi, *2D Metal Carbides and Nitrides (MXenes): Structure, Properties and Applications*, Springer Nature Switzerland AG, 2019.
51 S. Cao, Y. Hu, C. Yang, J. Li, H. Chen, S. Wei, S. Liu, Z. Wang, D. Sun and X. Lu, *J. CO_2 Util.*, 2022, **62**, 102074.
52 S. Larijani, A. Zarepour, A. Khosravi, S. Iravani, M. Eskandari and A. Zarrabi, *J. Mater. Chem. A*, 2025, **13**, 158–183.
53 J. Heo, N. Her, M. Jang, C. M. Park, A. Son, J. Han and Y. Yoon, *Crit. Rev. Environ. Sci. Technol.*, 2023, **53**, 987–1008.
54 J. Shen, Z. Wu, C. Li, C. Zhang, A. Genest, G. Rupprechter and L. He, *FlatChem*, 2021, **28**, 100252.
55 X. Liu, T. Chen, Y. Xue, J. Fan, S. Shen, M. S. A. Hossain, M. A. Amin, L. Pan, X. Xu and Y. Yamauchi, *Coord. Chem. Rev.*, 2022, **459**, 214440.
56 Y. Li, Y. Chen, Z. Guo, C. Tang, B. Sa, N. Miao, J. Zhou and Z. Sun, *Chem. Eng. J.*, 2022, **429**, 132171.
57 Y. Cheng, X. Xu, Y. Li, Y. Zhang and Y. Song, *Comput. Mater. Sci.*, 2022, **202**, 110971.
58 X. Zhu and Y. Li, *Wiley Interdiscip. Rev.: Comput. Mol. Sci.*, 2019, **9**, e1416.
59 N. H. Solangi, R. R. Karri, N. M. Mubarak and S. A. Mazari, *Process Saf. Environ. Prot.*, 2024, **185**, 1012–1037.
60 B. Wang, A. Zhou, F. Liu, J. Cao, L. Wang and Q. Hu, *J. Adv. Ceram.*, 2018, **7**, 237–245.
61 A. Arifutzzaman, I. N. Musa, M. K. Aroua and R. Saidur, *J. CO_2 Util.*, 2023, **68**, 102353.
62 N. Li, X. Chen, W.-J. Ong, D. R. MacFarlane, X. Zhao, A. K. Cheetham and C. Sun, *ACS Nano*, 2017, **11**, 10825–10833.
63 H. Li, L. Liu, T. Yuan, J. Zhang, T. Wang, J. Hou and J. Chen, *Nanoscale*, 2024, **16**, 11480–11495.
64 W. Bao, H. Shen, G. Zeng, Y. Zhang, Y. Wang, D. Cui, J. Xia, K. Jing, H. Liu and C. Guo, *Nanoscale*, 2025, **17**, 6204.
65 Q. Zhao, C. Zhang, R. Hu, Z. Du, J. Gu, Y. Cui, X. Chen, W. Xu, Z. Cheng and S. Li, *ACS Nano*, 2021, **15**, 4927–4936.
66 Y. Hao, F. Hu, S. Zhu, Y. Sun, H. Wang, L. Wang, Y. Wang, J. Xue, Y. F. Liao and M. Shao, *Angew. Chem., Int. Ed.*, 2023, **62**, e202304179.
67 F. Yu, Z. Zhou, Y. You, J. Zhan, T. Yao and L.-H. Zhang, *ACS Appl. Mater. Interfaces*, 2023, **15**, 24346–24353.
68 M. Abdinejad, S. Subramanian, M. K. Motlagh, M. Noroozifar, S. Duangdangchote, I. Neporozhnii, D. Ripepi, D. Pinto, M. Li and K. Tang, *Adv. Energy Mater.*, 2023, **13**, 2300402.
69 A. Athawale, B. M. Abraham, M. Jyothirmai and J. K. Singh, *J. Phys. Chem. C*, 2023, **127**, 24542–24551.
70 H. Jing, P. Zhao, C. Liu, Z. Wu, J. Yu, B. Liu, C. Su, W. Lei and Q. Hao, *ACS Appl. Mater. Interfaces*, 2023, **15**, 59524–59533.
71 Y. Cao, L. Liu, L. Wu, B. Yin and K. Wu, *ChemistrySelect*, 2025, **10**, e202405861.
72 A. S. Abdullahi, U. Mustapha, O. A. Taialla, E. Kotob, I. Hussain, K. Alhooshani, S. M. S. Jillani and S. A. Ganiyu, *J. Colloid Interface Sci.*, 2025, **692**, 137487.

© 2026 The Author(s). Published by the Royal Society of Chemistry

Open Access Article. Published on 23 February 2026. Downloaded on 4/9/2026 12:13:42 AM. This article is licensed under a Creative Commons Attribution-NonCommercial 3.0 Unported Licence.

73 J. Y. Kim, W. T. Hong, T. K. C. Phu, S. C. Cho, B. Kim, U. Baeck, H. S. Oh, J. H. Koh, X. Yu and C. H. Choi, *Adv. Sci.*, 2024, **11**, 2405154.
74 H. H. Cao, Z. H. He, P. P. Guo, Y. Tian, X. Wang, K. Wang, W. Wang, H. Wang, Y. Yang and Z. T. Liu, *ChemCatChem*, 2025, **17**, e202401133.
75 M. Krishnan, A. Vijayaprabhakaran and M. Kathiresan, *Nanoscale*, 2024, **16**, 16218–16226.
76 G. Wei, Z. Mao, L. Liu, T. Hao, L. Zhu, S. Xu, X. Wang and S. Tang, *ACS Appl. Mater. Interfaces*, 2024, **16**, 52233–52243.
77 N. Li, X. Wang, X. Lu, P. Zhang and W. J. Ong, *Chem.–Eur. J.*, 2021, **27**, 17900–17909.
78 Y. Zhang and Z. Cao, *J. Phys. Chem. C*, 2021, **125**, 13331–13342.
79 Y. Sun, X. Tan, X. Zhang, Y. Wang, Z. Ju and Q. Kang, *Colloids Surf., A*, 2025, **726**, 137808.
80 S. A. Farooqi, A. S. Farooqi, S. Sajjad, C. Yan and A. B. Victor, *Environ. Chem. Lett.*, 2023, **21**, 1515–1553.
81 S. Park, D. T. Wijaya, J. Na and C. W. Lee, *Catalysts*, 2021, **11**, 253.
82 J. Han, X. Bai, X. Xu, A. Husile, S. Zhang, L. Qi and J. Guan, *Chem. Sci.*, 2024, **15**, 7870–7907.
83 T. Lv, B. Wang and R. Wang, *Aerosol Air Qual. Res.*, 2022, **22**, 220227.
84 A. Kidanemariam, J. Lee and J. Park, *Polymers*, 2019, **11**, 2090.
85 H. V. Doan, H. Amer Hamzah, P. Karikkethu Prabhakaran, C. Petrillo and V. P. Ting, *Nano–Micro Lett.*, 2019, **11**, 54.
86 P. Silva, S. M. Vilela, J. P. Tomé and F. A. A. Paz, *Chem. Soc. Rev.*, 2015, **44**, 6774–6803.
87 A. Felix Sahayaraj, H. Joy Prabu, J. Maniraj, M. Kannan, M. Bharathi, P. Diwahar and J. Salamon, *J. Inorg. Organomet. Polym. Mater.*, 2023, **33**, 1757–1781.
88 J. Gandara-Loe, L. Pastor-Perez, L. Bobadilla, J. Odriozola and T. Reina, *React. Chem. Eng.*, 2021, **6**, 787–814.
89 S. Naghdi, A. Cherevan, A. Giesriegl, R. Guillet-Nicolas, S. Biswas, T. Gupta, J. Wang, T. Haunold, B. C. Bayer and G. Rupprechter, *Nat. Commun.*, 2022, **13**, 282.
90 S. A. E. Naser, K. O. Badmus and L. Khotseng, *Coatings*, 2023, **13**, 1456.
91 X. Shi, R. Shao, W. Huang, K. Li, Y. Chang, X. Pei and Z. Xu, *Fibers Polym.*, 2025, **26**, 463–494.
92 Y. Gao, Q. Wang, G. Ji, A. Li and J. Niu, *RSC Adv.*, 2021, **11**, 5361–5383.
93 V. Mishra and A. Mishra, in *Metal–Organic Frameworks as Forensic Detectors*, Springer, 2025, pp. 191–208.
94 A. Bagheri, S. Bellani, H. Beydaghi, Z. Wang, A. Morag, M. I. Zappia, J. K. Panda, S. Vaez, V. Mastronardi and A. Gamberini, *ChemSusChem*, 2025, **18**, e202401454.
95 Y. Wen, X. Zeng, Y. Xiao, W. Ruan, K. Xiong and Z. Lai, *Molecules*, 2024, **29**, 2320.
96 L. Ugwu, Y. Morgan and H. Ibrahim, *Chem. Eng. Commun.*, 2024, **211**, 1236–1261.
97 L. Jin and A. Seifitokaldani, *Catalysts*, 2020, **10**, 481.
98 C. Li, Y. Ji, Y. Wang, C. Liu, Z. Chen, J. Tang, Y. Hong, X. Li, T. Zheng and Q. Jiang, *Nano–Micro Lett.*, 2023, **15**, 113.
99 Y. Kamakura and D. Tanaka, *Chem. Lett.*, 2021, **50**, 523–533.
100 S. A. A. Razavi, W. Chen, H.-C. Zhou and A. Morsali, *Coord. Chem. Rev.*, 2024, **517**, 216004.
101 T. Shen, T. Liu, H. Mo, Z. Yuan, F. Cui, Y. Jin and X. Chen, *RSC Adv.*, 2020, **10**, 22881–22890.
102 S. Dutt, A. Kumar and S. Singh, *Clean Technol.*, 2023, **5**, 140–166.
103 Z. Han, Y. Yang, J. Rushlow, J. Huo, Z. Liu, Y.-C. Hsu, R. Yin, M. Wang, R. Liang and K.-Y. Wang, *Chem. Soc. Rev.*, 2025, **54**, 367–395.
104 X. Li, X. T. Wu, Q. Xu and Q. L. Zhu, *Adv. Mater.*, 2024, **36**, 2401926.
105 C. Jia, Y. Zhao, S. Song, Q. Sun, Q. Meyer, S. Liu, Y. Shen and C. Zhao, *Adv. Energy Mater.*, 2023, **13**, 2302007.
106 Z. Liu, M. Hou, M. Wang, W. Yang, Y. Han, Y. Zhao and Z. Shao, *Chem. Eng. J.*, 2025, **523**, 168095.
107 Z. Chen, Y. Guo, L. Han, J. Zhang, Y. Liu, J. Baeyens and Y. Lv, *Prog. Energy Combust. Sci.*, 2024, **104**, 101175.
108 Y. Han, H. Yang and X. Guo, *Synthesis Methods and Crystallization*, 2020, pp. 1–23.
109 S. Kumar, S. Jain, M. Nehra, N. Dilbaghi, G. Marrazza and K.-H. Kim, *Coord. Chem. Rev.*, 2020, **420**, 213407.
110 S. Shahzadi, M. Akhtar, M. Arshad, M. H. Ijaz and M. R. S. A. Janjua, *RSC Adv.*, 2024, **14**, 27575–27607.
111 J. F. Kurisingal, Y. Rachuri, Y. Gu, R. K. Chitumalla, S. Vuppala, J. Jang, K. K. Bisht, E. Suresh and D.-W. Park, *ACS Sustain. Chem. Eng.*, 2020, **8**, 10822–10832.
112 J. Niu, H. Li, L. Tao, Q. Fan, W. Liu and M. C. Tan, *ACS Appl. Mater. Interfaces*, 2023, **15**, 31664–31674.
113 H. Laeim, V. Molahalli, P. Prajongthat, A. Pattanaporkratana, G. Pathak, B. Phettong, N. Hongkarnjanakul and N. Chattham, *Polymers*, 2025, **17**, 130.
114 J. L. Obeso, M. T. Huxley, C. Leyva, J. G. Flores, N. Martín-Guaregua, M. Viniegra, J. Aguilar-Pliego, J. A. de los Reyes, I. A. Ibarra and R. A. Peralta, *Coord. Chem. Rev.*, 2023, **496**, 215403.
115 S. Zhou, T. Liu, M. Strømme and C. Xu, *Angew. Chem., Int. Ed.*, 2024, **63**, e202318387.
116 O. Ogunbanjo, P. Rodriguez and P. Anderson, *Mater. Chem. Front.*, 2025, **9**, 1650–1680.
117 J. Lu, Q. Wang, Z. Jin, Y. Xiao, B. H. Huang, C. H. Zhang, G. Z. Yang, Y. Zhou and F. S. Ke, *Chin. J. Chem.*, 2024, **42**, 2788–2794.
118 Y. Li and A. D. Chowdhury, *ChemCatChem*, 2025, **17**, e202401551.
119 J. Chen, M. R. Ahasan, J.-S. Oh, J. A. Tan, S. Hennessey, M. M. Kaid, H. M. El-Kaderi, L. Zhou, K. U. Lao and R. Wang, *J. Mater. Chem. A*, 2024, **12**, 4601–4609.
120 T.-V. Phuc, J.-S. Chung and S.-H. Hur, *Catalysts*, 2021, **11**, 537.
121 H. Yang, M. Zhang, Z. Guan and J. Yang, *Catal. Sci. Technol.*, 2023, **13**, 6238–6246.
122 C. Zhao, X. Dai, T. Yao, W. Chen, X. Wang, J. Wang, J. Yang, S. Wei, Y. Wu and Y. Li, *J. Am. Chem. Soc.*, 2017, **139**, 8078–8081.
123 Y. Zhang and W.-Y. Sun, *Chem. Commun.*, 2024, **60**, 8824–8839.

Open Access Article. Published on 23 February 2026. Downloaded on 4/9/2026 12:13:42 AM. This article is licensed under a Creative Commons Attribution-NonCommercial 3.0 Unported Licence.

124 C. Singh, S. Mukhopadhyay and I. Hod, *Nano Converg.*, 2021, **8**, 1.
125 C. Li, H. Yan, H. Yang, W. Zhou, C. Xie, B. Pan and Q. Zhang, *Sci. China Mater.*, 2025, **68**, 21–38.
126 Y. Wang, N.-Y. Huang, H.-Y. Wang, X.-W. Zhang, J.-R. Huang, P.-Q. Liao, X.-M. Chen and J.-P. Zhang, *CCS Chem.*, 2023, **5**, 145–151.
127 J. D. Yi, D. H. Si, R. Xie, Q. Yin, M. D. Zhang, Q. Wu, G. L. Chai, Y. B. Huang and R. Cao, *Angew. Chem.*, 2021, **133**, 17245–17251.
128 Z. Meng, J. Luo, W. Li and K. A. Mirica, *J. Am. Chem. Soc.*, 2020, **142**, 21656–21669.
129 S. Gu, J. Lu, X. Zhu, Y. Pan, T. Qi, D. Wang and J. Zhong, *Int. J. Hydrogen Energy*, 2025, **156**, 150353.
130 A. A. Zhang, Z. X. Wang, Z. B. Fang, J. L. Li and T. F. Liu, *Angew. Chem.*, 2024, **136**, e202412777.
131 S. K. Kurapati, in *Recent Advances in Materials Processing and Characterization: Select Proceedings of ICMPC 2021*, Springer, 2022, pp. 15–31.
132 G. Avci, C. Altintas and S. Keskin, *J. Phys. Chem. C*, 2021, **125**, 17311–17322.
133 Y. Zhang, L. Jiao, W. Yang, C. Xie and H. L. Jiang, *Angew. Chem., Int. Ed.*, 2021, **60**, 7607–7611.
134 Z.-Y. Jing, D.-H. Si, H. Guo, L.-L. Han, R. Cao and Y.-B. Huang, *CCS Chem.*, 2024, **6**, 3053–3064.
135 X. Yang, Q. X. Li, S. Y. Chi, H. F. Li, Y. B. Huang and R. Cao, *SmartMat*, 2022, **3**, 163–172.
136 L.-X. Liu, C. Qin, T. Deng, L. Sun, Z. Chen and X. Han, *J. Mater. Chem. A*, 2024, **12**, 26421–26438.
137 H. D. Singh, M. G, R. Misra, S. Sarkar, D. Chakraborty and S. Nandi, *Adv. Compos. Hybrid Mater.*, 2024, **7**, 209.
138 E. P. Delmo, Y. Wang, J. Wang, S. Zhu, T. Li, X. Qin, Y. Tian, Q. Zhao, J. Jang and Y. Wang, *Chin. J. Catal.*, 2022, **43**, 1687–1696.
139 L. S. Xie, G. Skorupskii and M. Dinca, *Chem. Rev.*, 2020, **120**, 8536–8580.
140 M. Wang, R. Dong and X. Feng, *Chem. Soc. Rev.*, 2021, **50**, 2764–2793.
141 C. Ma, Z. Wang, J. Li, M. Mu and X. Yin, *Electrochim. Acta*, 2023, **463**, 142774.
142 Z. Xin, J. Liu, X. Wang, K. Shen, Z. Yuan, Y. Chen and Y.-Q. Lan, *ACS Appl. Mater. Interfaces*, 2021, **13**, 54959–54966.
143 K. A. Adegoke and P. F. Tseki, *Carbon Capture Sci. Technol.*, 2025, **17**, 100523.
144 K.-G. Liu, F. Bigdeli, A. Panjehpour, A. Larimi, A. Morsali, A. Dhakshinamoorthy and H. Garcia, *Coord. Chem. Rev.*, 2023, **493**, 215257.
145 D. Yang and X. Wang, *SmartMat*, 2022, **3**, 54–67.
146 M. Guo, S. Du, G. Yang, Q. Zhang, Z. Liu and F. Peng, *Energy Fuels*, 2024, **38**, 11043–11050.
147 A. V. Rayer, E. Reid, A. Kataria, I. Luz, S. J. Thompson, M. Lail, J. Zhou and M. Soukri, *J. CO_2 Util.*, 2020, **39**, 101159.
148 X. Sun, A. I. O. Suarez, M. Meijerink, T. van Deelen, S. Ould-Chikh, J. Zečević, K. P. de Jong, F. Kapteijn and J. Gascon, *Nat. Commun.*, 2017, **8**, 1680.
149 A. H. Mamaghani, J. Liu, Z. Zhang, R. Gao, Y. Wu, H. Li, M. Feng and Z. Chen, *Adv. Energy Mater.*, 2024, **14**, 2402278.
150 Y. Huang, H. Zhu, Y. Wang, G. Yin, S. Chen, T. Li, C. Wu, S. Jia, J. Shang and Z. Ren, *Catalysts*, 2025, **15**, 936.
151 O. Ogunbanjo, P. Rodríguez and P. Anderson, *Mater. Chem. Front.*, 2025, **9**, 1650–1680.
152 Z. Li, Y. Lv, H. Huang, Z.-J. Li, T. Li, L. Zhang and J.-Q. Wang, *Dalton Trans.*, 2024, **53**, 7067–7072.
153 T. Van Phuc, S. G. Kang, J. S. Chung and S. H. Hur, *Mater. Res. Bull.*, 2021, **138**, 111228.
154 L. Jia, K. Wagner, J. Smyth, D. Officer, J. Chen and P. Wagner, *Polymers*, 2022, **14**, 5112.
155 J. Yang, H. Wu, Z. Wang, M. Lu, S. Liu, Z. Ren and Z. Chen, *Electrochim. Acta*, 2023, **441**, 141800.
156 R. K. Aparna, V. Surendran, D. Roy, B. Pathak, M. M. Shaijumon and S. Mandal, *ACS Appl. Energy Mater.*, 2023, **6**, 4072–4078.
157 Q. Wang, X. Yang, H. Zang, F. Chen, C. Wang, N. Yu and B. Geng, *Inorg. Chem.*, 2022, **61**, 12003–12011.
158 J. W. Lim, D. H. Choo, J. H. Cho, J. Kim, W. S. Cho, O. F. N. Okello, K. Kim, S. Lee, J. Son and S.-Y. Choi, *J. Mater. Chem. A*, 2024, **12**, 11090–11100.
159 W. Zhang, H. Li, D. Feng, C. Wu, C. Sun, B. Jia, X. Liu and T. Ma, *Carbon Energy*, 2024, **6**, e461.
160 C. J. Leverant, J. Cooper, D. F. Sava Gallis and J. A. Harvey, *J. Phys. Chem. C*, 2024, **128**, 16250–16257.
161 T. Paul, A. Juma, R. Alqerem, G. Karanikolos, H. A. Arafat and L. F. Dumée, *J. Environ. Chem. Eng.*, 2023, **11**, 111112.
162 M. Ding, X. Cai and H. Jiang, *Chem. Sci.*, 2019, **10**, 10209–10230.
163 X. Kang, B. Wang, K. Hu, K. Lyu, X. Han, B. F. Spencer, M. D. Frogley, F. Tuna, E. J. McInnes and R. A. Dryfe, *J. Am. Chem. Soc.*, 2020, **142**, 17384–17392.
164 X. Zhang, Y. Zhang, Q. Li, X. Zhou, Q. Li, J. Yi, Y. Liu and J. Zhang, *J. Mater. Chem. A*, 2020, **8**, 9776–9787.
165 Y. L. Yang, Y. R. Wang, L. Z. Dong, Q. Li, L. Zhang, J. Zhou, S. N. Sun, H. M. Ding, Y. Chen and S. L. Li, *Adv. Mater.*, 2022, **34**, 2206706.
166 S. Patel, K. McKelvey and L. Liu, *Chem. Mater.*, 2024, **36**, 10054–10087.
167 N. Gholampour, C. I. Ezugwu, H. A. Younus, D. P. Debecker, M. Al Abri, C.-M. Kao and F. Verpoort, *J. Mater. Chem. A*, 2024, **12**, 27825–27854.
168 J.-H. Li, Y.-S. Wang, Y.-C. Chen and C.-W. Kung, *Appl. Sci.*, 2019, **9**, 2427.
169 M. R. Thalji, F. Mahmoudi, L. G. Bachas and C. Park, *Int. J. Mol. Sci.*, 2025, **26**, 8019.
170 Z. Sun, R. Wang, V. E. Matulis and K. Vladimir, *Molecules*, 2024, **29**, 1286.
171 Samia, M. H. Jameel, M. Arain, I. Hussain, M. B. Hanif, S. Atri, M. Z. H. Mayzan and H. Dai, *Nano Mater. Sci.*, 2025, **7**, 444–481.
172 K. Huang, P. Qu, Y. Wang, C. Lian, J. Li, H. Su and H. Liu, *Ind. Eng. Chem. Res.*, 2023, **62**, 20716–20726.
173 H. Saini, N. Srinivasan, V. Šedajová, M. Majumder, D. P. Dubal, M. Otyepka, R. Zbořil, N. Kurra, R. A. Fischer and K. Jayaramulu, *ACS Nano*, 2021, **15**, 18742–18776.

© 2026 The Author(s). Published by the Royal Society of Chemistry

Open Access Article. Published on 23 February 2026. Downloaded on 4/9/2026 12:13:42 AM. This article is licensed under a Creative Commons Attribution-NonCommercial 3.0 Unported Licence.

174 H. Yang, G.-X. Zhang, H.-J. Zhou, Y.-Y. Sun and H. Pang, *Energy Mater. Adv.*, 2023, **4**, 0033.
175 Y. Tan, L. Yang, D. Zhai, L. Sun, S. Zhai, W. Zhou, X. Wang, W. Q. Deng and H. Wu, *Small*, 2022, **18**, 2204942.
176 G. Chellasamy, S. K. Arumugasamy, S. Kuppusamy, V. Ekambaram, K. Rajagopalan, S. Venkateswarlu, P. Deivasigamani, M. J. Choi, S. Govindaraju and K. Yun, *J. Mater. Chem. A*, 2024, **12**, 1115–1127.
177 X. Liu, X.-H. Liu, X. Zhang, H. Wang and Q. Zhao, *J. Mater. Chem. A*, 2024, **12**, 20578–20605.
178 M. Kashif, S. I. A. Shah, S. Khan, S. Ahmad, M. Anwar, S. U. Rahman, S. Azizi and M. Maaza, *Phys. Chem. Chem. Phys.*, 2025, **27**, 25204–25231.
179 P. Xiao, G. Zhu, X. Shang, B. Hu, B. Zhang, Z. Tang, J. Yang and J. Liu, *J. Electroanal. Chem.*, 2022, **916**, 116382.
180 Y. Li, Y. Liu, Z. Wang, P. Wang, Z. Zheng, H. Cheng, Y. Dai and B. Huang, *Chem. Eng. J.*, 2021, **411**, 128446.
181 L. Zhao, B. Dong, S. Li, L. Zhou, L. Lai, Z. Wang, S. Zhao, M. Han, K. Gao, M. Lu, X. Xie, B. Chen, Z. Liu, X. Wang, H. Zhang, H. Li, J. Liu, H. Zhang, X. Huang and W. Huang, *ACS Nano*, 2017, **11**, 5800–5807.
182 X. Nie, S. Wu, F. Huang, Q. Wang and Q. Wei, *ACS Appl. Mater. Interfaces*, 2021, **13**, 2245–2255.
183 W. Zhao, J. Peng, W. Wang, B. Jin, T. Chen, S. Liu, Q. Zhao and W. Huang, *Small*, 2019, **15**, 1901351.
184 X. Liang, X. Ren, Q. Yang, L. Gao, M. Gao, Y. Yang, H. Zhu, G. Li, T. Ma and A. Liu, *Nanoscale*, 2021, **13**, 2843–2848.
185 X. F. Lu, Y. Fang, D. Luan and X. W. D. Lou, *Nano Lett.*, 2021, **21**, 1555–1565.
186 J. Wang, T. Zhao, Z. Yang, Y. Chen, Y. Liu, J. Wang, P. Zhai and W. Wu, *ACS Appl. Mater. Interfaces*, 2019, **11**, 38654–38662.
187 L. Zhao, B. Dong, S. Li, L. Zhou, L. Lai, Z. Wang, S. Zhao, M. Han, K. Gao and M. Lu, *ACS Nano*, 2017, **11**, 5800–5807.
188 Y. Liu, Y. He, E. Vargun, T. Plachy, P. Saha and Q. Cheng, *Nanomaterials*, 2020, **10**, 695.
189 G. Nagaraju, S. C. Sekhar, B. Ramulu, S. K. Hussain, D. Narsimulu and J. S. Yu, *Nano–Micro Lett.*, 2021, **13**, 17.
190 C.-Y. Liu and E. Y. Li, *ACS Appl. Mater. Interfaces*, 2018, **11**, 1638–1644.
191 T. De Villenoisy, X. Zheng, V. Wong, S. S. Mofarah, H. Arandiyan, Y. Yamauchi, P. Koshy and C. C. Sorrell, *Adv. Mater.*, 2023, **35**, 2370174.
192 M. S. Challiwala, H. A. Choudhury, D. Wang, M. M. El-Halwagi, E. Weitz and N. O. Elbashir, *Sci. Rep.*, 2021, **11**, 1417.
193 Y. Xu, B. Liu, Y. Chen and S. Lu, *J. Environ. Manage.*, 2023, **347**, 119109.
194 Z. Li, J. Xiong, H. Song, S. Liu, Y. Huang, Y. Huang, G. I. Waterhouse, Z. Wang, Y. Mao and Z. Liang, *Sep. Purif. Technol.*, 2024, **341**, 126817.
195 M. Manikandan, P. Seyadu Abuthahir, S. Pachamuthu and E. Manikandan, *ACS Appl. Mater. Interfaces*, 2025, **17**, 51996–52009.
196 Z.-H. Zhu, X.-Y. Wu, J.-F. Lu, H. Xu, S.-L. Hou, J. Zhao, S.-J. Liu and H.-R. Wen, *Inorg. Chem.*, 2025, **64**, 8261–8269.
197 R. Saha, K. Gupta and C. J. Gómez García, *Cryst. Growth Des.*, 2024, **24**, 2235–2265.
198 X. Zhang, S. Zhang, Y. Tang, X. Huang and H. Pang, *Composites, Part B*, 2022, **230**, 109532.
199 F. Cao, Y. Zhang, H. Wang, K. Khan, A. K. Tareen, W. Qian, H. Zhang and H. Ågren, *Adv. Mater.*, 2022, **34**, 2107554.
200 P. Eghbali, A. Hassani, S. Wacławek, K.-Y. A. Lin, Z. Sayyar and F. Ghanbari, *Chem. Eng. J.*, 2024, **480**, 147920.
201 R. A. Soomro, P. Zhang, B. Fan, Y. Wei and B. Xu, *Nano–Micro Lett.*, 2023, **15**, 108.
202 Y. An, X. Lv, W. Jiang, L. Wang, Y. Shi, X. Hang and H. Pang, *Green Chem. Eng.*, 2024, **5**, 187–204.
203 M. S. Sajna, S. Zavahir, A. Popelka, P. Kasak, A. Al-Sharshani, U. Onwusogh, M. Wang, H. Park and D. S. Han, *J. Environ. Chem. Eng.*, 2023, **11**, 110467.
204 A. Iqbal, J. Hong, T. Y. Ko and C. M. Koo, *Nano Converg.*, 2021, **8**, 1–24.
205 Y. Shan, G. Zhang, Y. Shi and H. Pang, *Cell Rep. Phys. Sci.*, 2023, **4**, 101301.
206 T. Amrillah, C. A. Che Abdullah, A. Hermawan, F. N. Indah Sari and V. N. Alviani, *Nanomaterials*, 2022, **12**, 4280.
207 S. Iravani, *Ceram. Int.*, 2022, **48**, 24144–24156.
208 D. Chakraborty, A. Yurdusen, G. Mouchaham, F. Nouar and C. Serre, *Adv. Funct. Mater.*, 2024, **34**, 2309089.
209 V. F. Yusuf, N. I. Malek and S. K. Kailasa, *ACS Omega*, 2022, **7**, 44507–44531.
210 S. Verma, B. Kim, H. R. M. Jhong, S. Ma and P. J. Kenis, *ChemSusChem*, 2016, **9**, 1972–1979.
211 B. Endrodi, E. Kecsenovity, A. Samu, F. Darvas, R. Jones, V. Torok, A. Danyi and C. Janáky, *ACS Energy Lett.*, 2019, **4**, 1770–1777.
212 T. Burdyny and W. A. Smith, *Energy Environ. Sci.*, 2019, **12**, 1442–1453.
213 J. A. Rabinowitz and M. W. Kanan, *Nat. Commun.*, 2020, **11**, 5231.
214 P. De Luna, C. Hahn, D. Higgins, S. A. Jaffer, T. F. Jaramillo and E. H. Sargent, *Science*, 2019, **364**, eaav3506.
215 K. Sharma, V. Hasija, S. Patial, P. Singh, V.-H. Nguyen, A. K. Nadda, S. Thakur, P. Nguyen-Tri, C. C. Nguyen, S. Y. Kim, Q. V. Le and P. Raizada, *Int. J. Hydrogen Energy*, 2023, **48**, 6560–6574.
216 T. Amrillah, A. R. Supandi, V. Puspasari, A. Hermawan and Z. W. Seh, *Trans. Tianjin Univ.*, 2022, **28**, 307–322.

© 2026 The Author(s). Published by the Royal Society of Chemistry